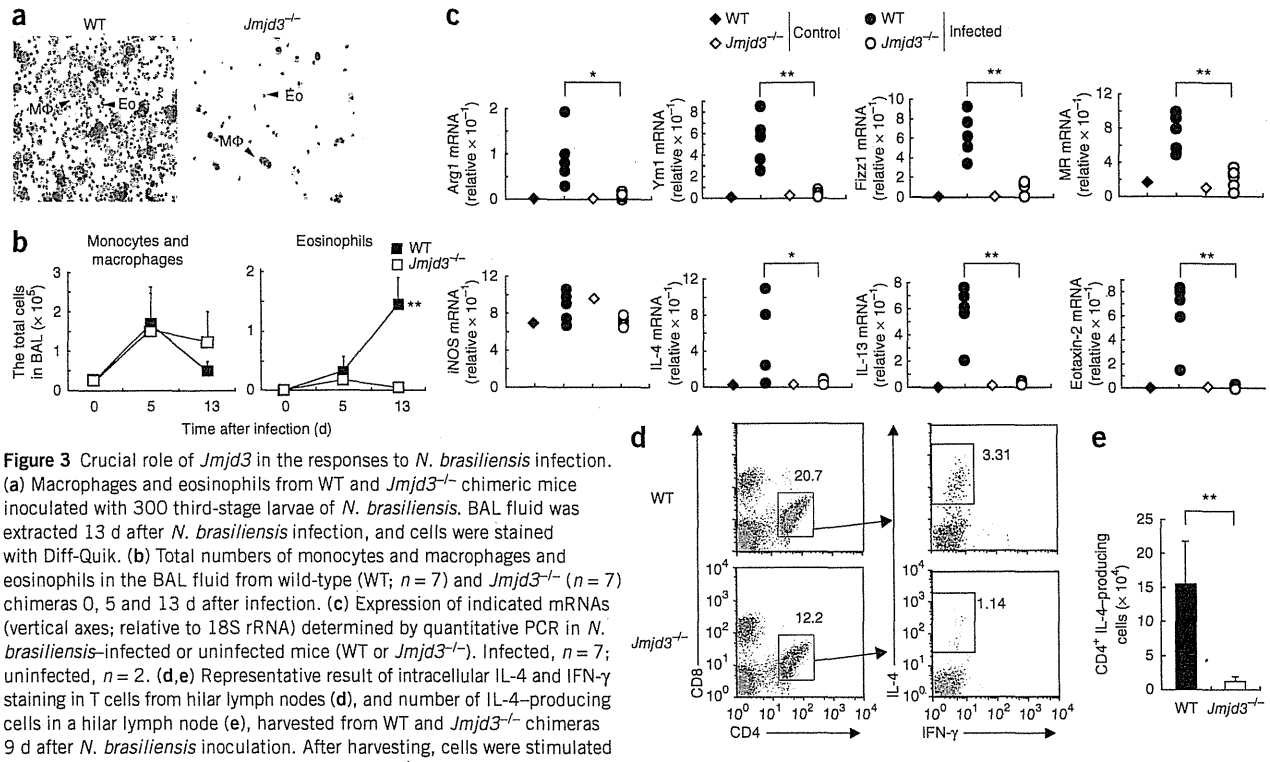

Figure 3 Crucial role of *Jmjd3* in the responses to *N. brasiliensis* infection. (**a**) Macrophages and eosinophils from WT and *Jmjd3*$^{-/-}$ chimeric mice inoculated with 300 third-stage larvae of *N. brasiliensis*. BAL fluid was extracted 13 d after *N. brasiliensis* infection, and cells were stained with Diff-Quik. (**b**) Total numbers of monocytes and macrophages and eosinophils in the BAL fluid from wild-type (WT; $n = 7$) and *Jmjd3*$^{-/-}$ ($n = 7$) chimeras 0, 5 and 13 d after infection. (**c**) Expression of indicated mRNAs (vertical axes; relative to 18S rRNA) determined by quantitative PCR in *N. brasiliensis*–infected or uninfected mice (WT or *Jmjd3*$^{-/-}$). Infected, $n = 7$; uninfected, $n = 2$. (**d**,**e**) Representative result of intracellular IL-4 and IFN-γ staining in T cells from hilar lymph nodes (**d**), and number of IL-4–producing cells in a hilar lymph node (**e**), harvested from WT and *Jmjd3*$^{-/-}$ chimeras 9 d after *N. brasiliensis* inoculation. After harvesting, cells were stimulated with CD3 and CD28 for 4 h, and CD4, CD8, IL-4 and IFN-γ expression were determined. Boxes and numbers indicate percentages of CD4$^+$ cells in hilar lymph node cells and IL-4–producing cells in CD4$^+$ cells. $^*P < 0.05$; $^{**}P < 0.01$ (two-tailed Student's *t*-test). Results are representative of two experiments with four mice per group (**a**,**b**), a single experiment with seven mice per group (**c**) or a single experiment with five mice (**d**,**e**) (error bars indicate s.d.).

However, the recruitment of eosinophils was severely impaired in *Jmjd3*$^{-/-}$ chimeric mice (**Fig. 3b**). To investigate the characteristics of recruited macrophages, we extracted RNA from lung tissue 5 d after *N. brasiliensis* infection. M2 markers such as Arg1, Ym1, Fizz1 and MR were barely expressed in *Jmjd3*$^{-/-}$ chimeras (**Fig. 3c**). Furthermore, induction of genes encoding the eosinophil-recruiting chemokine eotaxin-2 and the T_H2-inducing cytokines IL-4 and IL-13 was severely impaired in *Jmjd3*$^{-/-}$ chimeric mice (**Fig. 3c**). Thus, we

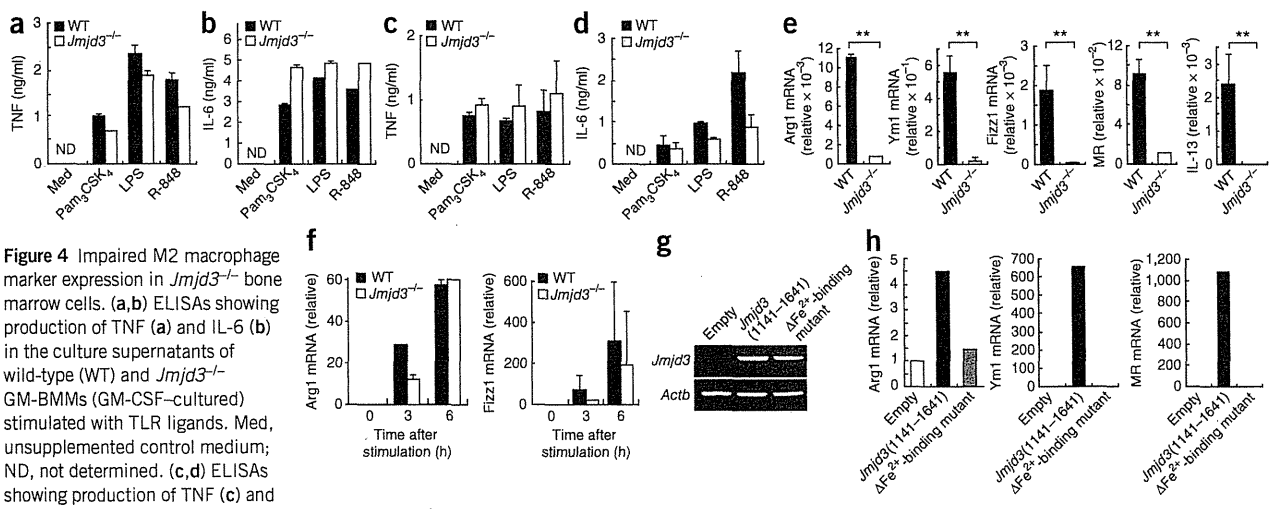

Figure 4 Impaired M2 macrophage marker expression in *Jmjd3*$^{-/-}$ bone marrow cells. (**a**,**b**) ELISAs showing production of TNF (**a**) and IL-6 (**b**) in the culture supernatants of wild-type (WT) and *Jmjd3*$^{-/-}$ GM-BMMs (GM-CSF–cultured) stimulated with TLR ligands. Med, unsupplemented control medium; ND, not determined. (**c**,**d**) ELISAs showing production of TNF (**c**) and IL-6 (**d**) in the culture supernatants of WT and *Jmjd3*$^{-/-}$ M-BMMs (M-CSF–cultured) stimulated with TLR ligands. (**e**) Quantitative PCR analysis showing expression of Arg1, Ym1, Fizz1, MR and IL-13 mRNAs (relative to 18S rRNA) in total RNA prepared from WT and *Jmjd3*$^{-/-}$ M-BMMs. (**f**) Quantitative PCR analysis showing expression of Arg1 and Fizz1 mRNAs (relative to 18S rRNA) in total RNA prepared from WT and *Jmjd3*$^{-/-}$ M-BMMs stimulated with IL-4 (10 ng/ml). (**g**,**h**) Reverse-transcription PCR showing expression of *Jmjd3* cDNA, with *Actb* cDNA as an expression control (**g**), and quantitative PCR showing expression of Arg1, Ym1 and MR mRNAs (relative to empty-vector control; **h**), in total RNA of *Jmjd3*$^{-/-}$ M-BMMs generated from bone marrow cells infected with retroviruses expressing WT Jmjd3 (amino acid residues 1141–1641) or its iron binding–deficient mutant. Results are representative of four (**a**–**d**), three (**e**,**f**) or two (**g**,**h**) independent experiments (error bars indicate s.d.).

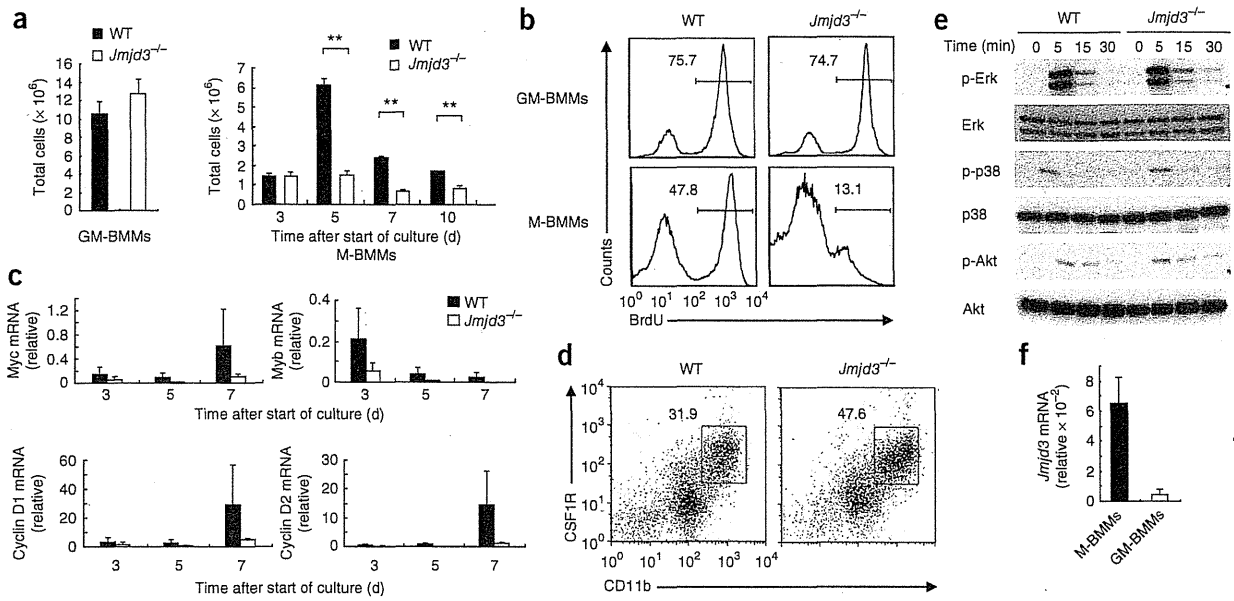

Figure 5 *Jmjd3* is required for the cell-cycle progression of M-BMMs. (**a**) Numbers of GM-BMMs and M-BMMs generated from wild-type (WT) and *Jmjd3*$^{-/-}$ bone marrow cells. Bone marrow cells from WT and *Jmjd3*$^{-/-}$ chimeras were cultured in the presence of GM-CSF for 5 d or M-CSF for time indicated (horizontal axis), and the number of adherent CD11b^{+} cells was counted. (**b**) Incorporation of BrdU in WT and *Jmjd3*$^{-/-}$ GM-BMMs and M-BMMs incubated in the presence of BrdU for 24 h. Incorporation was examined by intracellular staining with anti-BrdU. (**c**) Quantitative PCR showing expression of mRNAs encoding c-Myc, c-Myb, cyclin D1 and cyclin D2 (relative to 18S rRNA) in WT and *Jmjd3*$^{-/-}$ M-BMMs. (**d**) Surface expression of colony stimulating receptor (CSF1R) and CD11b on WT and *Jmjd3*$^{-/-}$ M-BMMs. Boxes and numbers indicate percentages of CSF1R-expressing M-BMMs. (**e**) Expression of phosphorylated (p-) and unphosphorylated Erk, p38 and Akt in WT and *Jmjd3*$^{-/-}$ M-BMMs stimulated with M-CSF (50 ng/ml). Cells were starved for 4 h before stimulation, and cell lysates were subjected to immunoblot analysis with antibodies to p-Erk, p-p38 and p-Akt. The membrane was stripped and reprobed for expression of Erk, p38 and Akt. (**f**) Quantitative PCR showing Jmjd3 mRNA expression (relative to 18S rRNA) by M-BMMs and GM-BMMs. $*P < 0.05$; $**P < 0.01$ (two-tailed Student's *t*-test). Results are representative of four (**a**), three (**b**,**f**) or two (**c**–**e**) independent experiments (error bars indicate s.d.).

investigated the activation of T cells in the pulmonary lymph nodes 9 d after *N. brasiliensis* infection. Whereas CD4^{+} T cells prepared from wild-type pulmonary lymph nodes expressed IL-4, but not IFN-γ, the frequency of IL-4–producing CD4^{+} T cells was severely impaired in pulmonary T cells prepared from *Jmjd3*$^{-/-}$ chimeric mice, suggesting that Jmjd3-mediated M2 macrophage activation is crucial for *N. brasiliensis* to induce T_H2 responses in the lung (**Fig. 3d**,**e**). However, histological changes in the intestine were not severely impaired in *Jmjd3*$^{-/-}$ chimeric mice (data not shown). Collectively, our results demonstrate that Jmjd3 is essential for mounting immune responses to helminth infection, directing M2 macrophage polarization in the lung but not in the small intestine.

Role of *Jmjd3* in M2 macrophage generation in response to M-CSF

Numerous studies have shown that GM-CSF induces M1 macrophages from bone marrow cells and M-CSF induces M2 macrophages from bone marrow cells[12–15]. When we used GM-CSF to generate macrophages, similar amounts of TNF and IL-6 were produced in wild-type and *Jmjd3*$^{-/-}$ chimeras in response to TLR ligands from adherent CD11b^{+} macrophages (termed GM-BMMs, for GM-CSF–induced bone marrow–derived macrophages; **Fig. 4a**,**b**). In contrast, production of IL-6, but not TNF, in response to TLR ligand stimulation was partially impaired in *Jmjd3*$^{-/-}$ bone marrow cultured in the presence of M-CSF (M-BMMs; **Fig. 4c**,**d**). Furthermore, the expression of genes encoding Arg1, Ym1, Fizz1, MR and IL-13 was severely impaired in M-BMMs from *Jmjd3*$^{-/-}$ chimeras (**Fig. 4e**), which indicates that *Jmjd3* is crucial for expression of hallmark M2 genes in M-BMMs. Jmjd3 is involved in the response of macrophages to IL-4 stimulation[34]; nevertheless, Arg1 and Fizz1 gene expression were similar after IL-4 stimulation in wild-type and *Jmjd3*$^{-/-}$ M-BMMs (**Fig. 4f**), suggesting that the responses to IL-4 were not impaired in *Jmjd3*$^{-/-}$ M-BMMs. We then used microarray analysis to examine the gene expression profiles in wild-type and *Jmjd3*$^{-/-}$ M-BMMs with or without LPS stimulation. The expression of 1,371 genes was more than 50% lower in unstimulated *Jmjd3*$^{-/-}$ M-BMMs compared with wild-type (**Supplementary Table 1**). In addition to *Arg1*, *Chi3l3* and *Fizz1*, the expression of cytokine genes such as *Il2*, *Il3*, *Il4*, *Il5* and *Il13*, as well as that of chemokine genes such as *Ccl1*, *Ccl17*, *Ccl22* and *Ccl24*, was severely impaired in *Jmjd3*$^{-/-}$ M-BMMs (**Supplementary Table 1**). The expression of 2,188 genes was more than twofold higher in wild-type M-BMMs in response to LPS stimulation, and that of 436 genes was reduced by over 50% in LPS-stimulated *Jmjd3*$^{-/-}$ M-BMMs (**Supplementary Table 2**). For example, the expression of *Il6* and *Il12b* was partially impaired in *Jmjd3*$^{-/-}$ M-BMMs, consistent with a previous report (**Supplementary Table 2**). Therefore, Jmjd3 is important for inducing expression of a large set of genes, and some of these are related to M2 macrophage polarization in M-BMMs.

In addition to its JmjC domain, Jmjd3 contains a putative tetratricopeptide repeat domain in the N terminus. We therefore examined whether the demethylase activity of Jmjd3 is needed for the defect in M2 macrophage marker expression. We retrovirally expressed the C-terminal part of Jmjd3, containing the JmjC domain (amino acid residues 1141–1641), or its iron binding–deficient mutant (A1388H) in *Jmjd3*$^{-/-}$ bone marrow cells and then induced M-BMMs (**Fig. 4g**).

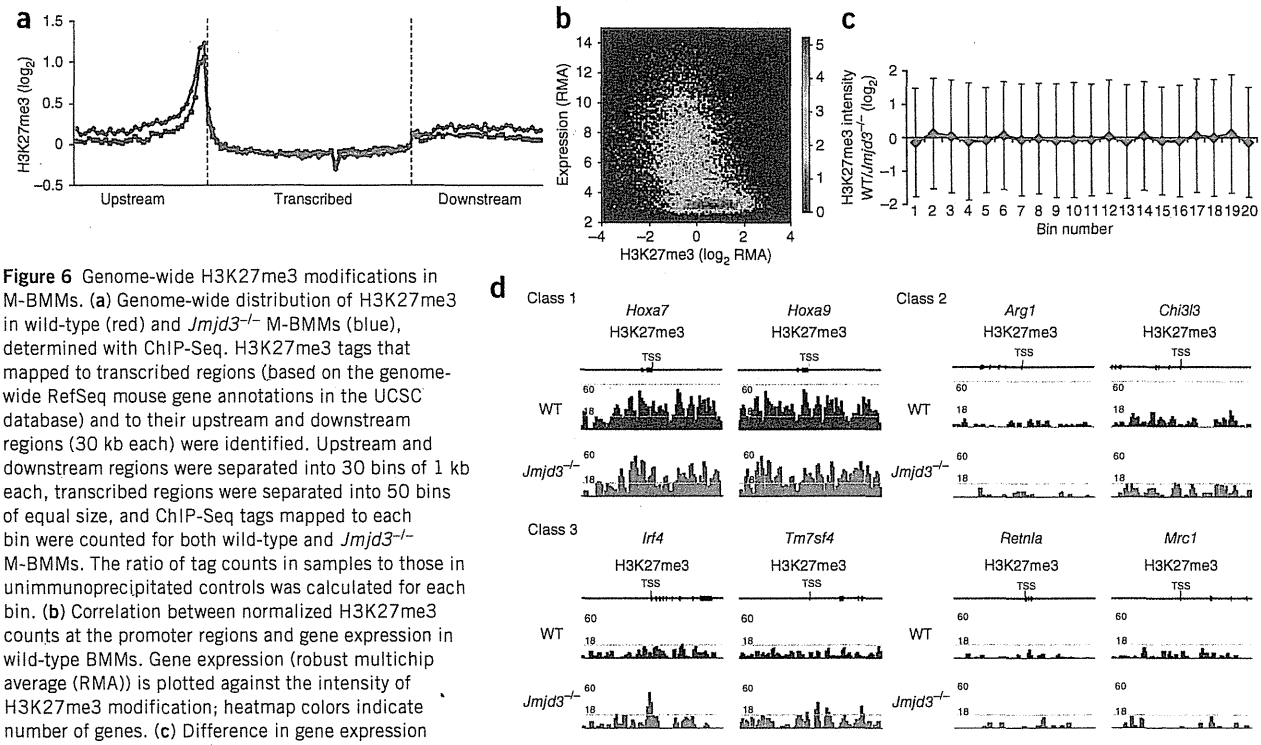

Figure 6 Genome-wide H3K27me3 modifications in M-BMMs. (**a**) Genome-wide distribution of H3K27me3 in wild-type (red) and *Jmjd3*$^{-/-}$ M-BMMs (blue), determined with ChIP-Seq. H3K27me3 tags that mapped to transcribed regions (based on the genome-wide RefSeq mouse gene annotations in the UCSC database) and to their upstream and downstream regions (30 kb each) were identified. Upstream and downstream regions were separated into 30 bins of 1 kb each, transcribed regions were separated into 50 bins of equal size, and ChIP-Seq tags mapped to each bin were counted for both wild-type and *Jmjd3*$^{-/-}$ M-BMMs. The ratio of tag counts in samples to those in unimmunoprecipitated controls was calculated for each bin. (**b**) Correlation between normalized H3K27me3 counts at the promoter regions and gene expression in wild-type BMMs. Gene expression (robust multichip average (RMA)) is plotted against the intensity of H3K27me3 modification; heatmap colors indicate number of genes. (**c**) Difference in gene expression between WT and *Jmjd3*$^{-/-}$ M-BMMs does not correlate with H3K27me3 levels. We classified RefSeq genes into 20 bins sorted by their expression difference between WT and *Jmjd3*$^{-/-}$ cells. Bins are numbered from low to high WT/*Jmjd3*$^{-/-}$ expression ratio. The average H3K27 modification intensity was calculated in each bin. (**d**) H3K27me3 modifications of wild-type (WT, blue) and *Jmjd3*$^{-/-}$ (red) cells on class 1 genes (*Hoxa7* and *Hoxa9*), class 2 genes (*Arg1*, *Chi3l3* for Ym1, *Fizz1*, *Mrc1* for MR) and class 3 genes (*Irf4* and *Tm7sf4*). Gray lines indicate the threshold tag counts for WT (18 tags) and *Jmjd3*$^{-/-}$ M-BMMs (18 tags) corresponding to a false discovery rate of 1×10^{-6}.

The A1388H mutation has been shown to abrogate the H3K27 demethylase activity of Jmjd3 (ref. 26). Expression of the C-terminal part of Jmjd3 was sufficient to upregulate M2 marker genes such as *Arg1*, *Chi3l3* and *Mrc1* (**Fig. 4h**). In contrast, the expression of *Jmjd3* (A1388H) did not increase the expression of M2 marker genes, which indicates that the H3K27me3 demethylase activity of Jmjd3 is necessary and sufficient for expression of M2 marker genes in M-BMMs.

M-BMMs require *Jmjd3* for cell cycle progression

In addition to the impaired M2 marker expression, the total number of M-BMM cells in *Jmjd3*$^{-/-}$ chimeras was considerably lower than in the wild type at days 5 and 7 of culture with M-CSF (**Fig. 5a**), although the number of GM-BMM cells (M1) was not altered. We found 5-bromodeoxyuridine (BrdU) incorporation, a measure of cell division, was severely impaired in *Jmjd3*$^{-/-}$ M-BMMs compared with wild-type cells (**Fig. 5b**), whereas wild-type and *Jmjd3*$^{-/-}$ GM-BMMs incorporated BrdU similarly. These results indicate that Jmjd3 controls cell-cycle progression in response to M-CSF stimulation. Expression of cell cycle–regulatory proteins (c-Myc, c-Myb, cyclin D1 and cyclin D2) was impaired in *Jmjd3*$^{-/-}$ M-BMMs at day 5 of culture (**Fig. 5c**); however, the surface expression of M-CSF receptor (CSF-1R) was normal in *Jmjd3*$^{-/-}$ M-BMMs (**Fig. 5d**). Furthermore, *Jmjd3* deficiency did not affect activation of the intracellular signaling molecules Erk, p38 and Akt, as indicated by their phosphorylation in M-BMMs (**Fig. 5e**), implying that the cell proliferation defects in *Jmjd3*$^{-/-}$ M-BMMs are not due to less activation of MAP kinases or Akt. The expression of *Jmjd3* in M-BMMs was much higher than that in GM-BMMs (**Fig. 5f**), suggesting that differential expression of *Jmjd3* in M-BMMs and GM-BMMs determines the contribution of Jmjd3 to their proliferation. Together, these data indicate that Jmjd3 performs a key step in the generation of M-BMMs, but not GM-BMMs, by controlling cell proliferation downstream of CSF-1R signaling.

Genome-wide analysis of H3K27me3 controlled by Jmjd3

Next we analyzed the genome-wide distribution of H3K27 trimethylation in wild-type and *Jmjd3*$^{-/-}$ M-BMMs by chromatin immunoprecipitation–sequencing (ChIP-Seq) analysis. We obtained an overall picture of the H3K27me3 distribution in transcribed regions (based on the genome-wide RefSeq mouse gene annotations in the University of California, Santa Cruz database) and in regions 30 kb upstream and 30 kb downstream. High levels of H3K27me3 tags were detected surrounding TSSs in M-BMMs from wild-type and *Jmjd3*$^{-/-}$ chimeras (**Fig. 6a**). In contrast, H3K27me3 levels were low in transcribed loci compared with upstream and downstream regions (**Fig. 6a**). Notably, H3K27me3 signals at the promoter and downstream regions were higher in *Jmjd3*$^{-/-}$ M-BMMs compared with wild-type cells.

We then compared the gene expression data obtained by microarray experiments with H3K27 methylation status. Overall, H3K27me3 levels in regions close to the TSS (−5 to +1 kb) correlated negatively with gene expression in M-BMMs (correlation coefficient −0.441; **Fig. 6b**). Next, we sorted genes by their ratio of expression in wild-type and *Jmjd3*$^{-/-}$ M-BMMs and examined H3K27me3 levels. However, we did not detect a correlation between H3K27me3 status and the difference in gene expression in wild-type compared with *Jmjd3*$^{-/-}$ M-BMMs (**Fig. 6c**). These data suggest that only small numbers of genes were affected by the absence of *Jmjd3*, and most loci are regulated by Utx or by both Jmjd3 and Utx.

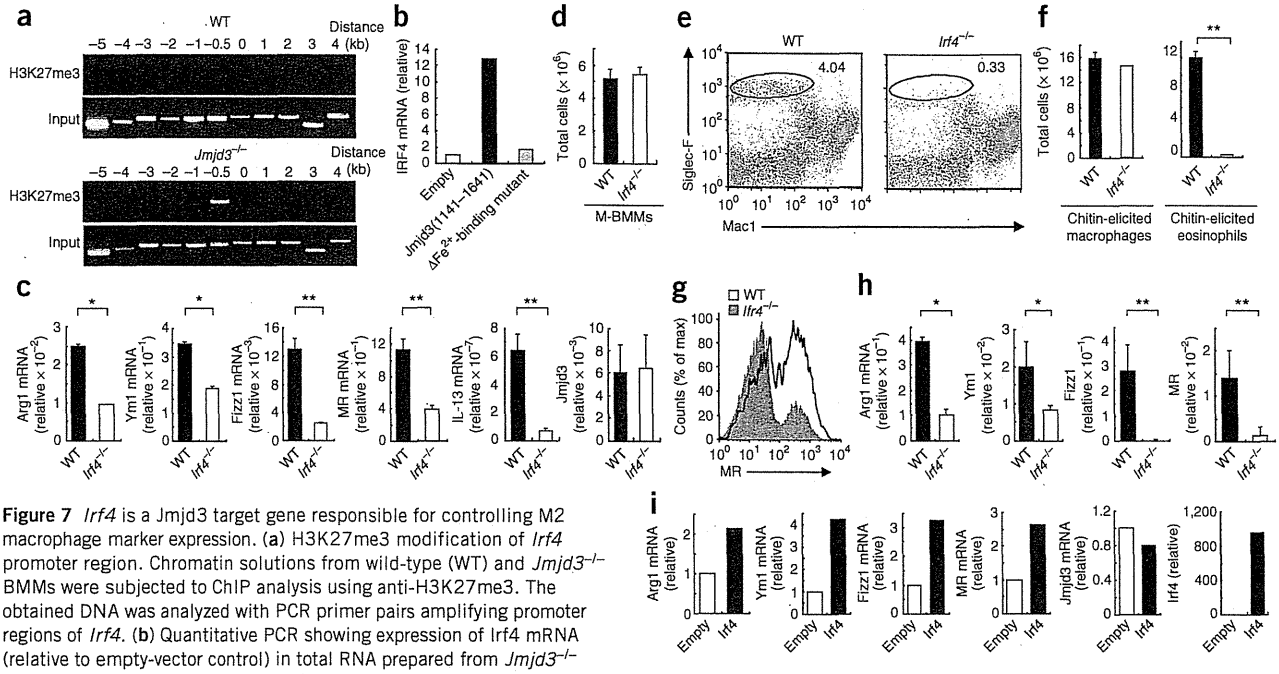

Figure 7 *Irf4* is a Jmjd3 target gene responsible for controlling M2 macrophage marker expression. (**a**) H3K27me3 modification of *Irf4* promoter region. Chromatin solutions from wild-type (WT) and *Jmjd3*$^{-/-}$ BMMs were subjected to ChIP analysis using anti-H3K27me3. The obtained DNA was analyzed with PCR primer pairs amplifying promoter regions of *Irf4*. (**b**) Quantitative PCR showing expression of Irf4 mRNA (relative to empty-vector control) in total RNA prepared from *Jmjd3*$^{-/-}$ M-BMMs retrovirally reconstituted with WT Jmjd3 (amino acid residues 1141–1641) or its iron binding–deficient mutant. (**c**) Quantitative PCR showing expression of M2 markers and Jmjd3 in bone marrow cells from WT and *Irf4*$^{-/-}$ mice cultured in the presence of M-CSF for 5 d. (**d**) Numbers of M-BMMs obtained from wild-type and *Irf4*$^{-/-}$ mice. (**e–g**) Macrophage and eosinophil recruitment (**e**), numbers of macrophages and eosinophils (**f**) and expression of MR (**g**) in macrophages from chitin-elicited PECs. WT and *Irf4*$^{-/-}$ mice were intraperitoneally treated with chitin, and PECs were prepared 48 h after treatment. Graph in **g** shows percentage of macrophages with the MR expression levels indicated on horizontal axis. (**h**) Quantitative PCR showing expression of M2 markers (relative to 18S rRNA) in total RNA prepared from PECs obtained from chitin-treated WT and *Irf4*$^{-/-}$ mice. (**i**) Quantitative PCR showing expression of M2 markers and Jmjd3 (relative to empty-vector control) in *Jmjd3*$^{-/-}$ M-BMMs in which Irf4 was ectopically expressed using retrovirus. $^{*}P < 0.05$; $^{**}P < 0.01$ (two-tailed Student's *t*-test). Results are representative of two (**a**,**b**,**i**) or three (**c–h**) independent experiments (error bars indicate s.d.).

Given the higher concentration of H3K27me3 tags in the region near the TSS, and the lack of overall correlation between expression changes and tag numbers, we focused on the promoter regions of individual genes that showed H3K27me3 peaks. We looked for peaks in wild-type and *Jmjd3*$^{-/-}$ M-BMM samples and divided the genome-wide set of genes into three different classes depending on H3K27me3 status (**Fig. 6d**). Class 1 genes harbored an H3K27me3 peak in wild-type M-BMMs. Class 2 genes did not have an H3K27me3 peak in either wild-type or *Jmjd3*$^{-/-}$ M-BMMs. Class 3 genes such as *Irf4* and *Tm7sf4* had an H3K27me3 peak in *Jmjd3*$^{-/-}$ but not in wild-type M-BMMs. We generated a table of 500 genes differentially expressed in wild-type and *Jmjd3*$^{-/-}$ M-BMMs, comparing H3K27 methylation status and gene expression from the microarray data (**Supplementary Table 3**).

Although *Hox* genes, such as *Hoxa7*, *Hoxa9* and *Tlx1* (also called *Hox11*), and *Bmp2* have been reported to be regulated by Jmjd3 (ref. 26), the H3K27 of their loci were highly trimethylated in M-BMMs both in the presence and absence of *Jmjd3*, and they therefore were assigned to class 1 (**Fig. 6d** and **Supplementary Table 3**). Furthermore, *Hox* and *Bmp2* gene expression was not lower in *Jmjd3*$^{-/-}$ M-BMMs (**Supplementary Table 3**), which indicates that these genes are not crucially regulated by Jmjd3 in M-BMMs. Furthermore, M2 marker genes, such as *Arg1*, *Chi3l3*, *Retnla* and *Mrc1*, were all in class 2, which indicates that their expression is not directly regulated by Jmjd3 (**Fig. 6d** and **Supplementary Table 3**). Thus, we proposed that transcription factors directly regulated by Jmjd3-mediated demethylation are responsible for the polarization of macrophages. When we searched genes categorized in class 3, we found *Irf4* and *Cebpb*. In particular, the promoter region close to the TSS of *Irf4* had a high H3K27me3 signal in *Jmjd3*$^{-/-}$ but not in wild-type M-BMMs (**Fig. 6d**).

Identification of *Irf4* as a Jmjd3 target gene

We confirmed by ChIP analysis that H3K27 at the promoter region of *Irf4* is differentially methylated in wild-type and *Jmjd3*$^{-/-}$ macrophages (**Fig. 7a**). Furthermore, when we retrovirally expressed the C-terminal region of Jmjd3 or its mutant in *Jmjd3*$^{-/-}$ macrophages, we found the expression of *Irf4* was demethylase activity dependent (**Fig. 7b**). These results demonstrate that *Irf4* is one of the Jmjd3 target genes in M-BMMs. Therefore, we examined the contribution of Irf4 to expression of mRNAs encoding Arg1, Ym1, Fizz1 and MR by using *Irf4*$^{-/-}$ mice. Induction of M2-related genes was severely impaired in *Irf4*$^{-/-}$ M-BMMs; in contrast, the expression of *Jmjd3* was similar between wild-type and *Irf4*$^{-/-}$ M-BMMs (**Fig. 7c**). Notably, the number of M-BMM cells was not lower in *Irf4*$^{-/-}$ mice (**Fig. 7d**). When chitin was administered peritoneally, recruitment of eosinophils, but not macrophages, was severely impaired in *Irf4*$^{-/-}$ mice (**Fig. 7e,f**). MR expression in chitin-elicited peritoneal macrophages was greatly impaired in *Irf4*$^{-/-}$ mice (**Fig. 7g**). In addition, the mRNA expression of the M2 macrophage markers encoding Arg1, Ym1, Fizz1 and MR was severely impaired in chitin-induced macrophages from *Irf4*$^{-/-}$ mice (**Fig. 7h**). These results demonstrate that Irf4 is crucial for the polarization of macrophages to M2 in M-BMMs and *in vivo* in response to chitin administration.

We then retrovirally expressed Irf4 in *Jmjd3*$^{-/-}$ M-BMMs and examined the expression of M2 marker genes (**Fig. 7i**). The expression

of Irf4 upregulated mRNAs encoding Arg1, Ym1, Fizz1 and MR in *Jmjd3*$^{-/-}$ M-BMMs, though the expression of Jmjd3 was unaltered (**Fig. 7i**). These results suggest that Irf4 contributes to the expression of M2 marker genes downstream of Jmjd3.

DISCUSSION

Here we focused on the role of Jmjd3 in macrophages mounting antibacterial and anti-parasitic responses. Whereas Jmjd3 was dispensable for M1 macrophage polarization, mice lacking *Jmjd3* did not mount proper M2 responses against helminth infection or chitin administration. Furthermore, bone marrow macrophages induced by M-CSF showed demethylase activity–dependent defects in expressing various genes, including M2 macrophage markers. Nevertheless, only a subset of genes had H3K27me3 levels differentially regulated by the presence or absence of *Jmjd3*. Among these genes, we found *Irf4* to be one of the direct targets of Jmjd3-mediated demethylation. Finally, we found that Irf4 is a transcription factor crucial for the induction of M2 macrophage responses.

Although *Jmjd3* is a TLR-inducible gene, *Jmjd3*$^{-/-}$ mice showed vigorous M1 macrophage activation in response to *Listeria* inoculation. These results suggest that *Jmjd3* is not essential for generating and recruiting M1 macrophages to bacterial infections. Our data are consistent with a previous report showing that gene expression in response to LPS stimulation is only modestly changed in macrophages lacking *Jmjd3* and that Jmjd3 in this case fine-tunes the transcriptional output[28]. TLR signaling upregulates genes involved not only in the promotion of inflammation, but also in termination or tissue remodeling. For instance, ATF3 and Zc3h12a are rapidly induced in response to TLR stimulation and inhibit inflammatory cytokine production[19,27]. It has been shown that M2 macrophages promote tissue remodeling as well as T_H2 responses. Thus, it is possible that *Jmjd3* induction functions as part of a feedback mechanism acting to repair inflammatory damage caused by TLR stimulation.

Chitin is an abundant structural component of helminths, crustaceans and fungi, and administration of chitin strongly induces M2 macrophage activation. Intraperitoneal administration of chitin recruited M2 macrophages and eosinophils in a Jmjd3- and Irf4-dependent fashion. These results indicate that the Jmjd3-*Irf4* axis is essential for M2 macrophage polarization to helminth infection.

However, addition of chitin to the macrophage culture did not stimulate the cells to upregulate M2 marker gene expression in our experiments (data not shown). Although TLR2 has been reported to mediate acute inflammation in response to chitin, another study has shown that chitin-mediated M2 macrophage activation is independent of MyD88, an adaptor molecule used by all TLRs (refs. 32,35). Currently, the mechanism by which chitin activates macrophages is not well understood. Moreover, it is still not clear what unique role Jmjd3 carries out in the generation of M2 macrophages in response to chitin and helminth infection. The identification of the chitin receptor(s) in the future will be vital for clarifying mechanisms of innate immune activation in response to helminth infection.

Jmjd3$^{-/-}$ mice also showed severe defects in recruiting M2 macrophages in response to *N. brasiliensis* infection. Although it is unknown which components of *N. brasiliensis* activate innate immune cells, Jmjd3-mediated H3K27me3 demethylation seems to be essential for macrophage responses to this parasite. Further studies are needed to identify the role of Jmjd3 in controlling infection with other helminths pathogenic to humans. M2 macrophages are known to be important for tumor cell survival and tissue remodeling in response to inflammation, in addition to the response against helminth infection[36]. Thus, it would be interesting to use this mouse model to explore how epigenetic regulation in macrophages promotes cancer progression or wound healing.

A previous report has found that *Jmjd3* expression is upregulated in response to IL-4 and that H3K27me3 levels decrease in response to IL-4 stimulation[34]. We observed that although M-BMMs and chitin-induced peritoneal macrophages showed severe defects in M2 macrophage marker expression in the absence of *Jmjd3*, *Jmjd3*$^{-/-}$ M-BMMs were capable of upregulating expression of genes representative of M2 macrophages in response to IL-4 stimulation. These findings suggest that IL-4 acts independently of Jmjd3-mediated H3K27 demethylation to promote M2 polarization. The same report[34] showed that H3K27me3 levels of various M2 marker genes were directly controlled by Jmjd3 to activate transcription. In contrast, our ChIP-Seq data demonstrate that H3K27me3 levels of most M2 marker genes, such as *Arg1*, are not changed in the absence of *Jmjd3*. Furthermore, deficiency in *Irf4*, one of the Jmjd3 target genes, resulted in defective M2 responses to chitin administration or M-CSF culture. Thus, it is more likely that Jmjd3 secondarily regulates M2 macrophage polarization by controlling expression of a set of transcription factors.

In addition to M2 marker gene expression, M-BMMs lacking *Jmjd3* showed proliferation defects in response to M-CSF stimulation. This is not due to impaired M-CSF receptor expression or defective activation of initial signaling molecules. Although the expression of genes involved in cell-cycle progression, such as those encoding c-Myc, cyclin D1 and cyclin D2, was impaired in *Jmjd3*$^{-/-}$ M-BMMs, H3K27me3 levels of these genes did not differ between wild-type and *Jmjd3*$^{-/-}$ M-BMMs. Furthermore, *Irf4*$^{-/-}$ M-BMMs did not show a defect in cell cycling (data not shown). Thus, it is possible that other Jmjd3 target genes are responsible for controlling the proliferation of M-BMMs.

ChIP-Seq analysis revealed that, in general, differences between wild-type and *Jmjd3*$^{-/-}$ M-BMM H3K27me3 levels at gene promoter regions were subtle. Nevertheless, gene expression profiles examined by microarray analysis were substantially different in wild-type and *Jmjd3*$^{-/-}$ M-BMMs, and the responses to chitin or helminth infection *in vivo* were severely impaired in *Jmjd3*$^{-/-}$ mice. Although it has been shown that *Hoxa* and *Bmp2* genes are potential targets of Jmjd3 (ref. 26), the expression of these genes was not lower in *Jmjd3*$^{-/-}$ cells, and the H3K27me3 levels were similar between wild-type and *Jmjd3*$^{-/-}$ M-BMMs. These results suggest that other H3K27 demethylases such as Utx and Uty compensate for the lack of *Jmjd3* in macrophages.

However, we identified Irf4 as one direct Jmjd3-specific target transcription factor. Irf4 has been shown to be involved in T_H2 cell polarization as well as in plasma cell differentiation and class-switch recombination in B cells[37,38]. It has also been reported that Irf4 functions in regulatory T cells to regulate T_H2 responses[39]. Indeed, *Irf4*$^{-/-}$ mice have been found to show defective T_H2 responses to *N. brasiliensis* infection[40]. Given that *Irf4*$^{-/-}$ mice did not induce M2 macrophages in response to chitin administration in our experiments, it is likely that the defects of macrophages in *Irf4*$^{-/-}$ mice also contribute to their abnormal responses to *N. brasiliensis* infection. In macrophages, Irf4 functions as a negative regulator of TLR signaling by associating with MyD88 (refs. 41,42).

Jmjd3$^{-/-}$ mice showed neonatal death due to a developmental defect in lung tissue. Although Jmjd3 directly regulated the expression of *Irf4* in macrophages, *Irf4*$^{-/-}$ mice did not show a developmental defect. Thus, Jmjd3 controls genes other than *Irf4* in the lung tissues for proper tissue development, and we focused solely on the role of this molecule in macrophages.

It is tempting to speculate that the change in epigenetic status is crucial for determining macrophage polarization. Future development of procedures to specifically regulate Jmjd3 demethylase activity might be useful for manipulating macrophages to mount anti-helminth host defenses and tissue repair.

METHODS

Methods and any associated references are available in the online version of the paper at http://www.nature.com/natureimmunology/.

Accession codes. GEO: microarray data, GSE23180; ChIP-Seq data, GSE23297.

Note: Supplementary information is available on the Nature Immunology website.

ACKNOWLEDGMENTS

We thank all the colleagues in our laboratory, E. Kamada for secretarial assistance and Y. Fujiwara, M. Kumagai, R. Abe, N. Kitagaki and S. Yumikura for technical assistance. This work was supported by the Special Coordination Funds of the Japanese Ministry of Education, Culture, Sports, Science and Technology, and grants from the Ministry of Health, Labour and Welfare in Japan, the Global Center of Excellence Programs of Osaka University and Nagasaki University and the US National Institutes of Health (P01 AI070167). Computational time was provided by the Super Computer System at the Human Genome Center, Institute of Medical Science, The University of Tokyo. A.V. was partly supported by a Japanese government scholarship.

AUTHOR CONTRIBUTIONS

T. Satoh and O.T. designed and performed experiments. Y.K., T. Miyake, K.M., T.O. and T. Saitoh performed experiments. A.V., Y.T., D.M.S. and K. Nakai analyzed ChIP-Seq data. K. Yasuda and K. Nakanishi performed *N. brasiliensis* infection experiments. K.H., T. Matsuyama and K. Yui provided *Irf4*$^{-/-}$ mice. T.T. performed histological examination. O.T., T. Satoh and S.A. wrote the manuscript. S.A. supervised the project. A.V. and K.Y. contributed equally to this work.

COMPETING FINANCIAL INTERESTS

The authors declare no competing financial interest.

Published online at http://www.nature.com/natureimmunology/.
Reprints and permissions information is available online at http://npg.nature.com/reprintsandpermissions/.

1. Takeuchi, O. & Akira, S. Pattern recognition receptors and inflammation. *Cell* **140**, 805–820 (2010).
2. Medzhitov, R. Origin and physiological roles of inflammation. *Nature* **454**, 428–435 (2008).
3. Beutler, B. Microbe sensing, positive feedback loops, and the pathogenesis of inflammatory diseases. *Immunol. Rev.* **227**, 248–263 (2009).
4. Mantovani, A., Sozzani, S., Locati, M., Allavena, P. & Sica, A. Macrophage polarization: tumor-associated macrophages as a paradigm for polarized M2 mononuclear phagocytes. *Trends Immunol.* **23**, 549–555 (2002).
5. Gordon, S. Alternative activation of macrophages. *Nat. Rev. Immunol.* **3**, 23–35 (2003).
6. Benoit, M., Desnues, B. & Mege, J.L. Macrophage polarization in bacterial infections. *J. Immunol.* **181**, 3733–3739 (2008).
7. Bronte, V. & Zanovello, P. Regulation of immune responses by L-arginine metabolism. *Nat. Rev. Immunol.* **5**, 641–654 (2005).
8. Nair, M.G., Guild, K.J. & Artis, D. Novel effector molecules in type 2 inflammation: lessons drawn from helminth infection and allergy. *J. Immunol.* **177**, 1393–1399 (2006).
9. Nair, M.G. *et al.* Chitinase and Fizz family members are a generalized feature of nematode infection with selective upregulation of Ym1 and Fizz1 by antigen-presenting cells. *Infect. Immun.* **73**, 385–394 (2005).
10. Stein, M., Keshav, S., Harris, N. & Gordon, S. Interleukin 4 potently enhances murine macrophage mannose receptor activity: a marker of alternative immunologic macrophage activation. *J. Exp. Med.* **176**, 287–292 (1992).
11. Mantovani, A. *et al.* The chemokine system in diverse forms of macrophage activation and polarization. *Trends Immunol.* **25**, 677–686 (2004).
12. Verreck, F.A. *et al.* Human IL-23-producing type 1 macrophages promote but IL-10-producing type 2 macrophages subvert immunity to (myco)bacteria. *Proc. Natl. Acad. Sci. USA* **101**, 4560–4565 (2004).
13. Martinez, F.O., Gordon, S., Locati, M. & Mantovani, A. Transcriptional profiling of the human monocyte-to-macrophage differentiation and polarization: new molecules and patterns of gene expression. *J. Immunol.* **177**, 7303–7311 (2006).
14. Fleetwood, A.J., Lawrence, T., Hamilton, J.A. & Cook, A.D. Granulocyte-macrophage colony-stimulating factor (CSF) and macrophage CSF-dependent macrophage phenotypes display differences in cytokine profiles and transcription factor activities: implications for CSF blockade in inflammation. *J. Immunol.* **178**, 5245–5252 (2007).
15. Fleetwood, A.J., Dinh, H., Cook, A.D., Hertzog, P.J. & Hamilton, J.A. GM-CSF- and M-CSF-dependent macrophage phenotypes display differential dependence on type I interferon signaling. *J. Leukoc. Biol.* **86**, 411–421 (2009).
16. Medzhitov, R. & Horng, T. Transcriptional control of the inflammatory response. *Nat. Rev. Immunol.* **9**, 692–703 (2009).
17. Yamamoto, M. *et al.* Regulation of Toll/IL-1-receptor-mediated gene expression by the inducible nuclear protein IκBζ. *Nature* **430**, 218–222 (2004).
18. Kayama, H. *et al.* Class-specific regulation of pro-inflammatory genes by MyD88 pathways and IκBζ. *J. Biol. Chem.* **283**, 12468–12477 (2008).
19. Gilchrist, M. *et al.* Systems biology approaches identify ATF3 as a negative regulator of Toll-like receptor 4. *Nature* **441**, 173–178 (2006).
20. Charo, I.F. Macrophage polarization and insulin resistance: PPARγ in control. *Cell Metab.* **6**, 96–98 (2007).
21. Wei, G. *et al.* Global mapping of H3K4me3 and H3K27me3 reveals specificity and plasticity in lineage fate determination of differentiating CD4+ T cells. *Immunity* **30**, 155–167 (2009).
22. Barski, A. *et al.* High-resolution profiling of histone methylations in the human genome. *Cell* **129**, 823–837 (2007).
23. Schuettengruber, B., Chourrout, D., Vervoort, M., Leblanc, B. & Cavalli, G. Genome regulation by polycomb and trithorax proteins. *Cell* **128**, 735–745 (2007).
24. Hong, S. *et al.* Identification of JmjC domain-containing UTX and JMJD3 as histone H3 lysine 27 demethylases. *Proc. Natl. Acad. Sci. USA* **104**, 18439–18444 (2007).
25. Lan, F. *et al.* A histone H3 lysine 27 demethylase regulates animal posterior development. *Nature* **449**, 689–694 (2007).
26. De Santa, F. *et al.* The histone H3 lysine-27 demethylase Jmjd3 links inflammation to inhibition of polycomb-mediated gene silencing. *Cell* **130**, 1083–1094 (2007).
27. Matsushita, K. *et al.* Zc3h12a is an RNase essential for controlling immune responses by regulating mRNA decay. *Nature* **458**, 1185–1190 (2009).
28. De Santa, F. *et al.* Jmjd3 contributes to the control of gene expression in LPS-activated macrophages. *EMBO J.* **28**, 3341–3352 (2009).
29. Barradas, M. *et al.* Histone demethylase JMJD3 contributes to epigenetic control of INK4a/ARF by oncogenic RAS. *Genes Dev.* **23**, 1177–1182 (2009).
30. Agger, K. *et al.* The H3K27me3 demethylase JMJD3 contributes to the activation of the INK4A-ARF locus in response to oncogene- and stress-induced senescence. *Genes Dev.* **23**, 1171–1176 (2009).
31. Bowman, S.M. & Free, S.J. The structure and synthesis of the fungal cell wall. *Bioessays* **28**, 799–808 (2006).
32. Reese, T.A. *et al.* Chitin induces accumulation in tissue of innate immune cells associated with allergy. *Nature* **447**, 92–96 (2007).
33. Kreider, T., Anthony, R.M., Urban, J.F. Jr. & Gause, W.C. Alternatively activated macrophages in helminth infections. *Curr. Opin. Immunol.* **19**, 448–453 (2007).
34. Ishii, M. *et al.* Epigenetic regulation of the alternatively activated macrophage phenotype. *Blood* **114**, 3244–3254 (2009).
35. Da Silva, C.A., Hartl, D., Liu, W., Lee, C.G. & Elias, J.A. TLR-2 and IL-17A in chitin-induced macrophage activation and acute inflammation. *J. Immunol.* **181**, 4279–4286 (2008).
36. Mantovani, A. & Sica, A. Macrophages, innate immunity and cancer: balance, tolerance, and diversity. *Curr. Opin. Immunol.* **22**, 231–237 (2010).
37. Ahyi, A.N., Chang, H.C., Dent, A.L., Nutt, S.L. & Kaplan, M.H. IFN regulatory factor 4 regulates the expression of a subset of T_H2 cytokines. *J. Immunol.* **183**, 1598–1606 (2009).
38. Klein, U. *et al.* Transcription factor IRF4 controls plasma cell differentiation and class-switch recombination. *Nat. Immunol.* **7**, 773–782 (2006).
39. Zheng, Y. *et al.* Regulatory T-cell suppressor program co-opts transcription factor IRF4 to control T_H2 responses. *Nature* **458**, 351–356 (2009).
40. Honma, K. *et al.* Interferon regulatory factor 4 differentially regulates the production of T_H2 cytokines in naive vs. effector/memory CD4+ T cells. *Proc. Natl. Acad. Sci. USA* **105**, 15890–15895 (2008).
41. Honma, K. *et al.* Interferon regulatory factor 4 negatively regulates the production of proinflammatory cytokines by macrophages in response to LPS. *Proc. Natl. Acad. Sci. USA* **102**, 16001–16006 (2005).
42. Negishi, H. *et al.* Negative regulation of Toll-like-receptor signaling by IRF-4. *Proc. Natl. Acad. Sci. USA* **102**, 15989–15994 (2005).

ONLINE METHODS

Generation of *Jmjd3*$^{-/-}$ mice. The *Jmjd3* gene was isolated from genomic DNA extracted from embryonic stem cells (GSI-I) by PCR. The targeting vector was constructed by replacing a 4-kb fragment encoding the *Jmjd3* open reading frame (exons 14–21, including exons encoding the JmjC domain) with a neomycin-resistance gene cassette (*neo*), and herpes simplex virus thymidine kinase was inserted into the genomic fragment for negative selection. After the targeting vector was transfected into embryonic stem cells, G418 and gancyclovir doubly-resistant colonies were selected and screened by PCR; recombination was further confirmed by Southern blotting. These homologous-recombinant clones were microinjected into blastocysts derived from C57BL/6 mice and were transferred to pseudopregnant females. Matings of chimeric male mice to C57BL/6 female mice resulted in transmission of the mutant allele to the germline. Resulting *Jmjd3*$^{+/-}$ mice were intercrossed to generate *Jmjd3*$^{-/-}$ mice. All animal experiments were done with the approval of the Animal Research Committee of the Research Institute for Microbial Diseases, Osaka University.

Mice, cells and reagents. *Irf4*$^{-/-}$ mice were prepared as described[41]. Bone marrow–derived macrophages were generated in RPMI-1640 medium containing 10% (vol/vol) FCS, 50 μM 2-mercaptoethanol and 10 ng/ml GM-CSF (PeproTech) or 10 ng/ml M-CSF (PeproTech). Pam_3CSK_4 and R-848 were prepared as described[27]. LPS (*Salmonella minnesota* Re595) was from Sigma.

Generation of bone marrow–chimeric mice. Fetal liver cells were prepared from wild-type and *Jmjd3*$^{-/-}$ embryos (embryonic day 15.5). The cell suspensions were intravenously injected into lethally irradiated CD45.1 C57BL/6 mice. The chimeric mice were given neomycin and ampicillin in their drinking water for 4 weeks. The mice were analyzed at least 8 weeks after reconstitution. More than 90% of splenocytes from chimeric mice were CD45.2 positive.

Quantitative PCR analysis. Total RNA was isolated with TRIzol (Invitrogen), and reverse transcription was performed with ReverTra Ace (Toyobo) according to the manufacturer's instructions. For quantitative PCR, cDNA fragments were amplified by Realtime PCR Master Mix (Toyobo); fluorescence from the TaqMan probe for each cytokine was detected by a 7500 real-time PCR system (Applied Biosystems). To determine the relative induction of cytokine mRNA in response to various stimuli, the mRNA expression level of each gene was normalized to the expression level of 18S rRNA. The experiments were repeated at least twice.

Immunoblot analysis. M-BMMs were cultured for 4 h in medium without M-CSF (PeproTech) and then were collected and replated. M-BMMs were stimulated with M-CSF for times indicated in **Figure 5e** and were lysed with lysis buffer (20 mM Tris-HCl, pH 7.5, 150 mM NaCl, 1 mM EDTA and 1% (vol/vol) Nonidet P-40) containing complete mini protease inhibitor cocktail (Roche). Cell lysates were separated by standard SDS-PAGE and analyzed by immunoblot. Antibodies to the following proteins were used: phosphorylated Erk (Cell Signaling no. 9101), phosphorylated Akt (Cell Signaling 9271), phosphorylated p38 (Cell Signaling 9211), Akt (Cell Signaling 9272), p38 (Santa Cruz C-20), Erk (Santa Cruz K-23) and β-actin (Santa Cruz C-11).

Flow cytometry. Antibodies for flow cytometry were purchased from BD Biosciences and eBioscience. Cells were washed in ice-cold flow-cytometry buffer (2% (vol/vol) FCS and 2 mM EDTA in PBS, pH 7.5), then incubated with each antibody for 15 min and washed twice with flow-cytometry buffer. Intracellular cytokines were stained with Cytofix/Cytoperm Plus Fixation/Permeabilization Kit (BD Biosciences) according to the manufacturer's instructions. Data were acquired on a FACSCalibur flow cytometer (BD Biosciences) and analyzed with FlowJo (Tree Star).

Construction of *Jmjd3* expression plasmids. *Jmjd3* cDNA (corresponding to amino acid residues 1141–1641) was obtained by PCR from a mouse cDNA library, and a point mutation resulting in the A1388H substitution in the JmjC domain was introduced by site-directed mutagenesis (Stratagene). The full or mutated *Jmjd3* cDNAs were cloned into the pMRX-ires-puro vector for retrovirus production[43].

Retroviral transduction. Bone marrow cells were isolated from *Jmjd3*$^{-/-}$ mice that had been injected intraperitoneally 4 d earlier with 5 mg of 5-fluorouracil (Nacalai Tesque). Cells were cultured in stem cell medium (RPMI supplemented with 15% (vol/vol) FCS, 10 mM sodium pyruvate, 2 μM L-glutamine, 50 μM β-mercaptoethanol, 100 U/ml penicillin, 100 g/ml streptomycin, 100 ng/ml stem cell factor, 10 ng/ml IL-6 and 10 ng/ml IL-3). Then, 48 h later, these cells were transduced with retroviral supernatant (supplemented with stem cell factor, IL-6, IL-3 and 10 ng/ml of polybrene) on two successive days. Virus was produced by PlatE packaging cells transfected with various plasmids. After the second transduction, cells were washed and resuspended in macrophage growth medium (RPMI-1640 medium supplemented with 10% (vol/vol) FCS, 50 μM β-mercaptoethanol, 100 U/ml penicillin, 100 μg/ml streptomycin and 20 ng/ml M-CSF). After 3.5 d in culture, cells were washed once and macrophage growth medium with 2.5 μg/ml puromycin (InvivoGen) was added. The cells were cultivated for 2 d after changing of the medium and then were analyzed.

Chitin administration. Chitin (Sigma) was washed three times in PBS and then sonicated with a UR-20P device (Tomy) for 30 min on ice. After filtration with 100 μM cell strainer, chitin was diluted in 50 ml PBS. About 800 ng chitin was intraperitoneally injected, and PECs were collected 2 d after administration.

Responses to *N. brasiliensis* infection. Wild-type and *Jmjd3*$^{-/-}$ fetal liver–chimeric mice were subcutaneously inoculated with 300 third-stage larvae of *N. brasiliensis* 8 weeks after fetal liver transfer. On day 5 after infection, *N. brasiliensis*–inoculated mice were killed and perfused with PBS, and total RNAs from lungs were extracted. RNA was subjected to quantitative PCR for the analysis of expression of various genes. Nine days after infection, hilar lymph nodes were harvested, a single-cell suspension was prepared and cell numbers were counted. The lymph node cells were stimulated with anti-CD3 and anti-CD28. They were stained with CD4 and treated with cytofix (BD Biosciences), then stained with anti–IL-4 and anti–IFN-γ. Next, the cells were examined by flow cytometry. BAL was performed at 5 and 13 d after *N. brasiliensis* infection, and macrophages and eosinophils were enumerated on cytospin smears stained with Diff-Quick (Baxter Healthcare).

Microarray and chromatin immunoprecipitation–sequencing analysis. Microarray and ChIP-Seq protocols and data analysis are described in **Supplementary Methods**.

Statistics. Statistical significance was calculated with the two-tailed Student's *t*-test.

43. Saitoh, T. *et al.* TWEAK induces NF-κB2 p100 processing and long lasting NF-κB activation. *J. Biol. Chem.* **278**, 36005–36012 (2003).

Virus-Infection or 5′ppp-RNA Activates Antiviral Signal through Redistribution of IPS-1 Mediated by MFN1

Kazuhide Onoguchi[1,2,3], Koji Onomoto[1], Shiori Takamatsu[1,2], Michihiko Jogi[1,2], Azumi Takemura[1], Shiho Morimoto[1], Ilkka Julkunen[4], Hideo Namiki[3], Mitsutoshi Yoneyama[5,6], Takashi Fujita[1,2]*

1 Department of Molecular Genetics, Institute for Virus Research, Kyoto University, Kyoto, Japan, **2** Graduate School of Biostudies, Kyoto University, Yoshida-Konoe Sakyo, Kyoto, Japan, **3** Graduate School of Science and Engineering, Waseda University, Tokyo, Japan, **4** Department of Vaccination and Immune Protection, National Institute for Health and Welfare, Helsinki, Finland, **5** Division of Molecular Immunology, Medical Mycology Research Center, Chiba University, Chuo-ku, Chiba, Japan, **6** PRESTO, Japan Science and Technology Agency, Saitama, Japan

Abstract

In virus-infected cells, RIG-I-like receptor (RLR) recognizes cytoplasmic viral RNA and triggers innate immune responses including production of type I and III interferon (IFN) and the subsequent expression of IFN-inducible genes. Interferon-β promoter stimulator 1 (IPS-1, also known as MAVS, VISA and Cardif) is a downstream molecule of RLR and is expressed on the outer membrane of mitochondria. While it is known that the location of IPS-1 is essential to its function, its underlying mechanism is unknown. Our aim in this study was to delineate the function of mitochondria so as to identify more precisely its role in innate immunity. In doing so we discovered that viral infection as well as transfection with 5′ppp-RNA resulted in the redistribution of IPS-1 to form speckle-like aggregates in cells. We further found that Mitofusin 1 (MFN1), a key regulator of mitochondrial fusion and a protein associated with IPS-1 on the outer membrane of mitochondria, positively regulates RLR-mediated innate antiviral responses. Conversely, specific knockdown of MFN1 abrogates both the virus-induced redistribution of IPS-1 and IFN production. Our study suggests that mitochondria participate in the segregation of IPS-1 through their fusion processes.

Citation: Onoguchi K, Onomoto K, Takamatsu S, Jogi M, Takemura A, et al. (2010) Virus-Infection or 5′ppp-RNA Activates Antiviral Signal through Redistribution of IPS-1 Mediated by MFN1. PLoS Pathog 6(7): e1001012. doi:10.1371/journal.ppat.1001012

Editor: C. Cheng Kao, Indiana University, United States of America

Received February 17, 2010; **Accepted** June 18, 2010; **Published** July 22, 2010

Funding: The Ministry of Education, Culture, Sports, Science and Technology of Japan (http://www.mext.go.jp/english/), the Ministry of Health, Labour and Welfare of Japan (http://www.mhlw.go.jp/english/index.html), the PRESTO Japan Science and Technology Agency (http://www.jst.go.jp/kisoken/presto/index_e.html), the Uehara Memorial Foundation (http://www.ueharazaidan.com/), the Mochida Memorial Foundation for Medical and Pharmaceutical Research (http://www.mochida.co.jp/zaidan/l), and Nippon Boehringer Ingelheim (http://www.boehringer-ingelheim.co.jp/com/Home/index.jsp). The funders had no role in study design, data collection and analysis, decision to publish, or preparation of the manuscript.

Competing Interests: The authors have declared that no competing interests exist.

* E-mail: tfujita@virus.kyoto-u.ac.jp

Introduction

Type I and III interferons (IFNs) play central roles in innate immune responses to viral infections [1,2,3,4]. In a variety of tissues, IFN production is triggered by a cytoplasmic sensor, retinoic acid inducible gene I (RIG-I)-like Receptor (RLR), which specifically senses viral RNA and induces antiviral signaling [5,6]. Once RLR is activated, its signal is relayed through physical interaction to IFN-β promoter stimulator 1 (IPS-1, also known as MAVS, VISA or Cardif) [7,8,9,10]. IPS-1 interacts with multiple signal transducers and protein kinases that activate transcription factors to induce IFN and other cytokine genes [11]. IPS-1 is expressed on the mitochondrial outer membrane and this localization is essential for signaling to occur [9]. However the reason for this underlying mechanism is unknown. Here, we investigated the cellular distribution of IPS-1 in virus-infected cells. We observed that IPS-1 is usually distributed evenly in all mitochondria in uninfected cells, however upon viral infection or the introduction of 5′ppp-RNA, which mimics viral RNA [12,13,14], a redistribution of IPS-1 occurred, resulting in a speckle-like pattern on mitochondria. Furthermore, we demonstrated that a mitochondrial GTPase, Mitofusin 1 (MFN1), which regulates mitochondrial fission and fusion [15], plays a critical role in the redistribution of IPS-1, as well as in virus-induced IFN production. Our study highlights the novel mitochondrial regulatory function of specifically sorting IPS-1 and providing a signaling platform for antiviral responses.

Results

Dynamic redistribution of IPS-1 in virus-infected or 5′ppp-RNA-transfected cells

To examine the localization of IPS-1 during viral infections, we generated HeLa cell lines stably expressing FLAG-tagged IPS-1 (IPS-1-HeLa clones, Fig. 1). Although the temporary expression of wild type (wt) IPS-1 results in constitutive signaling [7,8,9,10], the stable cell lines did not exhibit the constitutive activation of downstream target genes. However, upon infection with the Sendai virus (SeV), the cells exhibited increased expression of IFN and chemokine genes (*IFNB1*, *IL29*, *IL28A*, *IL28B* and *CXCL11*) and interferon-stimulated genes (*DDX58*, *IFIH1*, *DHX58*, *IFIT1-3*, and *OASL*) (Fig. 1B and C). Furthermore, the IPS-1-HeLa clones exhibited diminished susceptibility to Encephalomyocarditis virus (EMCV) replication (1 to 2 log) (Fig. 1D). The low basal activity and elevated signaling after SeV-infection suggest that FLAG-IPS-1 is under a regulatory control similar to that of endogenous IPS-1.

Author Summary

Virus-infections, such as influenza and chronic hepatitis C, are prominent diseases and outbreaks of newly emerging viruses are serious problems for modern society. Higher animals, including humans, are genetically equipped with mechanisms, collectively known as innate immunity, to counteract viral infections. RIG-I-like receptor (RLR), a cytoplasmic sensor, contributes to immune regulation by detecting infections by RNA viruses and triggering a series of responses which results in the activation of innate antiviral genes. Furthermore, it has been demonstrated that IPS-1, the adaptor protein of RLR, is expressed on mitochondrial outer membrane. Mitochondrion is an organelle of prokaryotic cell origin; it regulates energy production, and is involved in cell growth and cell death. Why IPS-1 is located on the mitochondrial outer membrane and how mitochondria are involved in antiviral signaling are yet to be explained clearly. In this report, we discovered that mitochondrial fusion protein MFN1 plays a novel function to mediate IPS-1 redistribution, which appears to be a critical step in RLR signaling.

Like endogenous IPS-1, FLAG-tagged IPS-1 is expressed on mitochondria in uninfected cells as shown by co-staining with MitoTracker (Fig. 2A, Mock). However, compared to the even cytoplasmic staining in the mock-infected cells, the staining pattern of IPS-1 became noticeably speckled in SeV-infected cells (Fig. 2A, SeV). Quantification of the fluorescence image revealed that mitochondria heavily stained with MitoTracker but lightly stained with anti-FLAG antibody were produced in SeV-infected cells. This redistribution was also observed with another mitochondrial marker, endoplasmic reticulum-associated amyloid β-peptide-binding protein (ERAB) (Fig. 2B), and different viruses (Newcastle disease virus (NDV), Sindbis virus, EMCV, Influenza virus, and Vesicular stomatitis virus (VSV)) (Fig. 3).

We also examined the distribution of IPS-1 in 5′ppp-RNA-transfected cells. Unlike synthetic single stranded RNA (5′OH-RNA), 5′ppp-RNA is a chemical ligand for RIG-I and is known to mimic viral signaling [12,13,14]. Interestingly, as with a viral infection, 5′ppp-RNA induced a redistribution of IPS-1, suggesting that the redistribution was triggered through RIG-I signaling. It is worth noting that EMCV, which selectively activates another RLR, melanoma differentiation-associated gene 5 (MDA5), also caused the redistribution of IPS-1, suggesting that this effect is common to RLRs. We suspected that IPS-1-HeLa cells exhibit enhanced redistribution of IPS-1 due to enhanced signaling (>10 IFN-β mRNA accumulation, Fig. 1B). This led us to analyze the distribution pattern of endogenous IPS-1 in HeLa cells, and we observed that the distribution pattern of endogenous IPS-1 changed in SeV-infected cells, although exclusive staining by mitochondrial marker was not observed (Fig. 4A). Similar to IPS-1-HeLa cells, we observed that hepatocellular carcinoma SKHep1 cells NDV, SeV, Influenza virus, or Sindbis virus infection also induced a speckled staining pattern in endogenous IPS-1 (Fig. 4B), and displayed enhanced IRF-3 dimerization when compared with HeLa cells (our unpublished data). This suggests that the redistribution is not simply an artifact due to the overexpression of FLAG-IPS-1.

Localization of viral nucleocapsid, RIG-I, and IPS-1

In order to activate RLR signaling, we used NDV to infect cells because it is available an anti-nucleocapsid protein (NP) antibody, a probe for the viral RNA-NP complex. NDV infection resulted in foci of NP in the cytoplasm and induced foci of RIG-I to form (Fig. 5A) [16]. RIG-I was evenly distributed in the cytoplasm, however some of the foci co-localized with those of NP (Fig. 5A). A similar formation of foci and co-localization with viral nucleoprotein complex was observed with other viruses (Ko.O. unpublished observations). IPS-1 accumulated on the periphery of the foci of RIG-I (Fig. 5B) and NP (Fig. 5C). We speculate that activated RIG-I recruits IPS-1, because RIG-I and IPS-1 interacted with each other through CARD-CARD interaction [7,8]. IPS-1 did not co-localize with RIG-I nor NP presumably because mitochondria do not penetrate these foci nor is IPS-1 released from mitochondria. Immunoelectron microscopy using the anti-NP antibody clearly identified the NP foci (Fig. 6A), and anti-FLAG staining (Fig. 6B) showed that mitochondrial IPS-1 accumulated on the periphery of NP foci in NDV infected cells.

A dominant negative mutant of RIG-I does not induce IPS-1 redistribution

To determine if the observed redistribution of IPS-1 is functionally relevant, we used a point mutant of RIG-I (K270A), which normally recognizes ligand RNA but functions as a dominant negative inhibitor (Fig. 7A) [14]. It was observed that NDV infection induced foci of both wt and K270A RIG-I to form (Fig. 7B), however wt but not K270A promoted the speckled staining pattern of IPS-1 (Fig. 7C). The results indicate that the redistribution of IPS-1 is strongly correlated with the activation of antiviral signaling.

Mitofusin 1, but not Mitofusin 2, plays a critical role in RIG-I-induced antiviral signaling

RIG-I was originally identified by screening an expression cDNA library [17]. In addition to the cDNA encoding RIG-I, there were several other candidate cDNA clones which enhance virus-responsive reporter activity. Two of the independent clones encoded a full-length protein, Mitofusin 1 (MFN1). Human MFN1 is composed of 741 amino acids and domains of GTPase and transmembranes (Fig. 8A). MFN1 together with its related protein Mitofusin 2 (MFN2) is expressed on the outer membrane of mitochondria and regulates mitochondrial dynamics [18,19]. Hyper- and hypo-functioning of either MFN1 or MFN2 result in elongated/aggregated and fragmented mitochondria, respectively. GTPase activity was previously shown to be essential for mitochondrial morphological change, particularly the fragmentation of mitochondria induced by a GTP-binding-deficient mutant of MFN1 (MFN1 T109A) [18].

Consistent with the screening results, overexpression of MFN1, but not MFN2, augmented IFN-β promoter activity (Fig. 8B). The GTPase activity is involved in this MFN1 function, since MFN1 T109A significantly inhibited the signaling induced by NDV or 5′ppp-RNA (Fig. 8C and D). It is worth noting that overexpression of MFN1, which results in elongated mitochondria, is not by itself sufficient to deliver the signal. To confirm that the increased signaling observed by MFN1 overexpression was correlated with RIG-I activation, we transfected cells with a combination of RIG-I and MFN1. The RIG-I/MFN1 combination showed enhanced IFN-β promoter activity, but the RIG-I K270A mutant/MFN1 combination failed to do so (Fig. 8E). MEFs derived from mice with disrupted *Mfn1* or *Mfn2* gene was used to confirm the specific involvement of MFN1 in virus-induced antiviral signaling (Fig. 9A and B). The results indicated that MFN1, but not MFN2, is essential for the signal transduction mediated by RIG-I.

We examined other regulatory proteins for mitochondrial fission/fusion mechanism. Optic atrophy protein 1 (OPA1) is

A

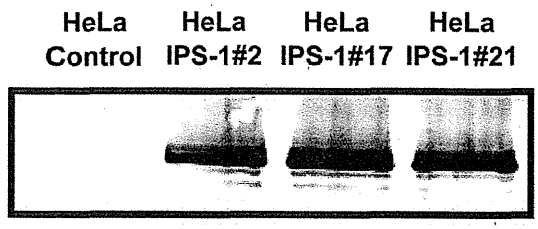

B

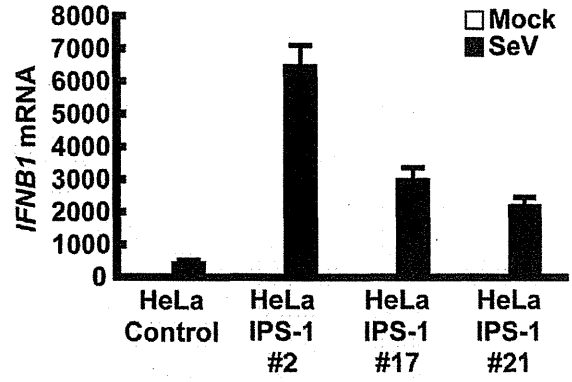

C

	HeLa Control		HeLa IPS-1#2		HeLa IPS-1#17	
	Mock	SeV	Mock	SeV	Mock	SeV
IL29	1.0	3.6	0.8	18.2	0.7	7.2
IL28A	1.0	2.0	0.7	11.7	0.6	6.9
IL28B	1.0	3.4	0.8	23.9	0.7	12.8
DDX58	1.0	1.1	0.7	1.8	0.7	3.8
IFIH1	1.0	2.3	0.8	5.1	1.8	8.8
DHX58	1.0	1.5	0.7	2.4	0.7	3.1
IFIT1	1.0	21.3	1.1	51.0	7.4	65.1
IFIT2	1.0	11.7	1.0	27.0	1.5	32.3
IFIT3	1.0	9.2	0.9	29.8	2.8	43.3
OASL	1.0	5.9	1.2	20.5	2.3	29.9
CXCL11	1.0	2.7	0.7	10.6	1.2	15.9

>9.0
6.0~8.9
3.0~5.9
1.4~2.9
0.7~1.3
<0.6

D

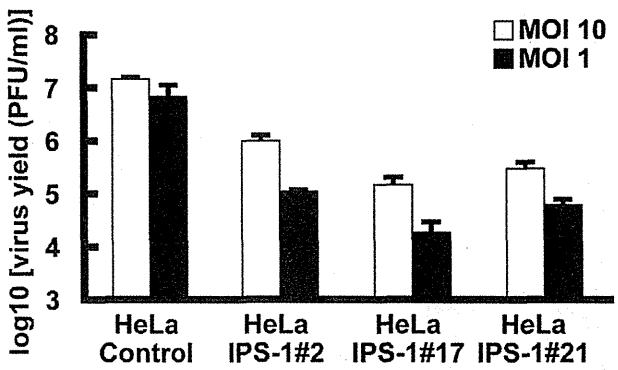

Figure 1. Stable HeLa cell clones expressing FLAG tagged IPS-1. A, Expression of FLAG-IPS-1 was examined in control and IPS-1-expressing HeLa clones (#2, 17, and 21) by immunoblotting using anti-FLAG antibody. **B**, Expression of *IFNB1* in control and IPS-1-HeLa cells was examined by quantitative real time PCR (qRT-PCR). Open and filled bars indicate mock-treated and SeV-infected cells for 12 h, respectively. Data represent means ± s.d. (n = 3). **C**, Expression profiles of cytokine and chemokine genes in control and IPS-1-HeLa cells. Total RNA extracted from indicated cells mock-treated or SeV-infected for 12 h was subjected to analysis using a DNA microarray. Relative mRNA levels using a control expression of 1.0 are shown. **D**, Replication of EMCV in control and IPS-1-HeLa clones. The indicated cell clones were infected with EMCV at a MOI of 1 or 10. The viral titer in the culture medium at 24 h post-infection was determined with the plaque assay. Data represent means ± s.d. (n = 3).
doi:10.1371/journal.ppat.1001012.g001

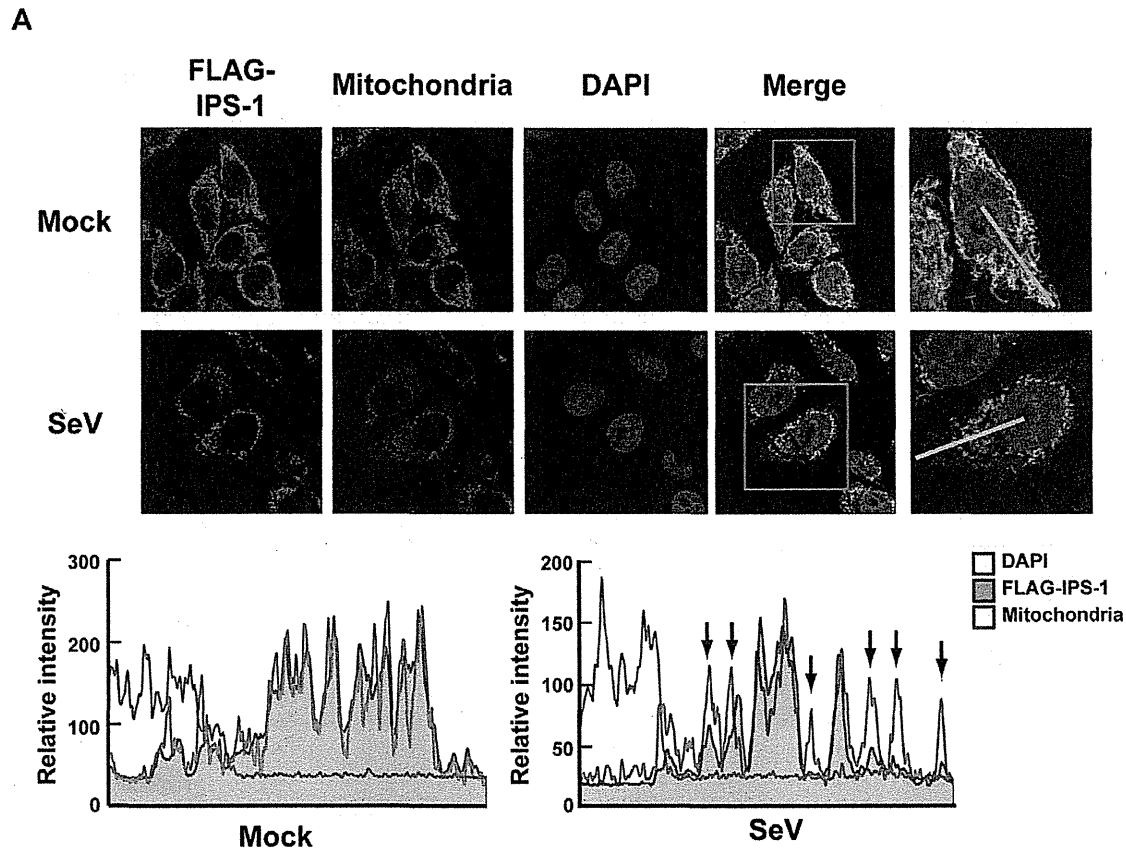

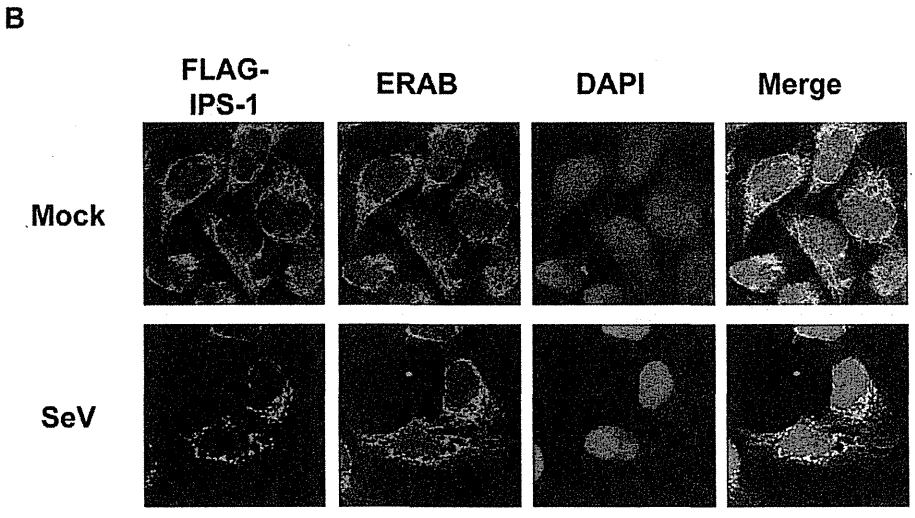

Figure 2. Redistribution of IPS-1 in SeV-infected cells. A, The IPS-1-HeLa clone #2 was mock-treated or infected with SeV for 12 h and stained with MitoTracker (Mitochondria) and anti-FLAG antibody (FLAG-IPS-1). Nuclei were visualized by staining with DAPI throughout this study. The fluorescent image was quantified in the area indicated by blue line (right most panel). Quantification results from mock- or SeV-infected cells are shown at the bottom. Fluorescence of DAPI corresponds to area in the nucleus. The mitochondria heavily stained with MitoTracker but lightly stained with anti-FLAG are shown by arrows. **B,** IPS-1-HeLa cells were mock-treated or infected with SeV for 12 h. Cells were stained with anti-FLAG antibody (FLAG-IPS-1) and anti-ERAB antibody (ERAB).
doi:10.1371/journal.ppat.1001012.g002

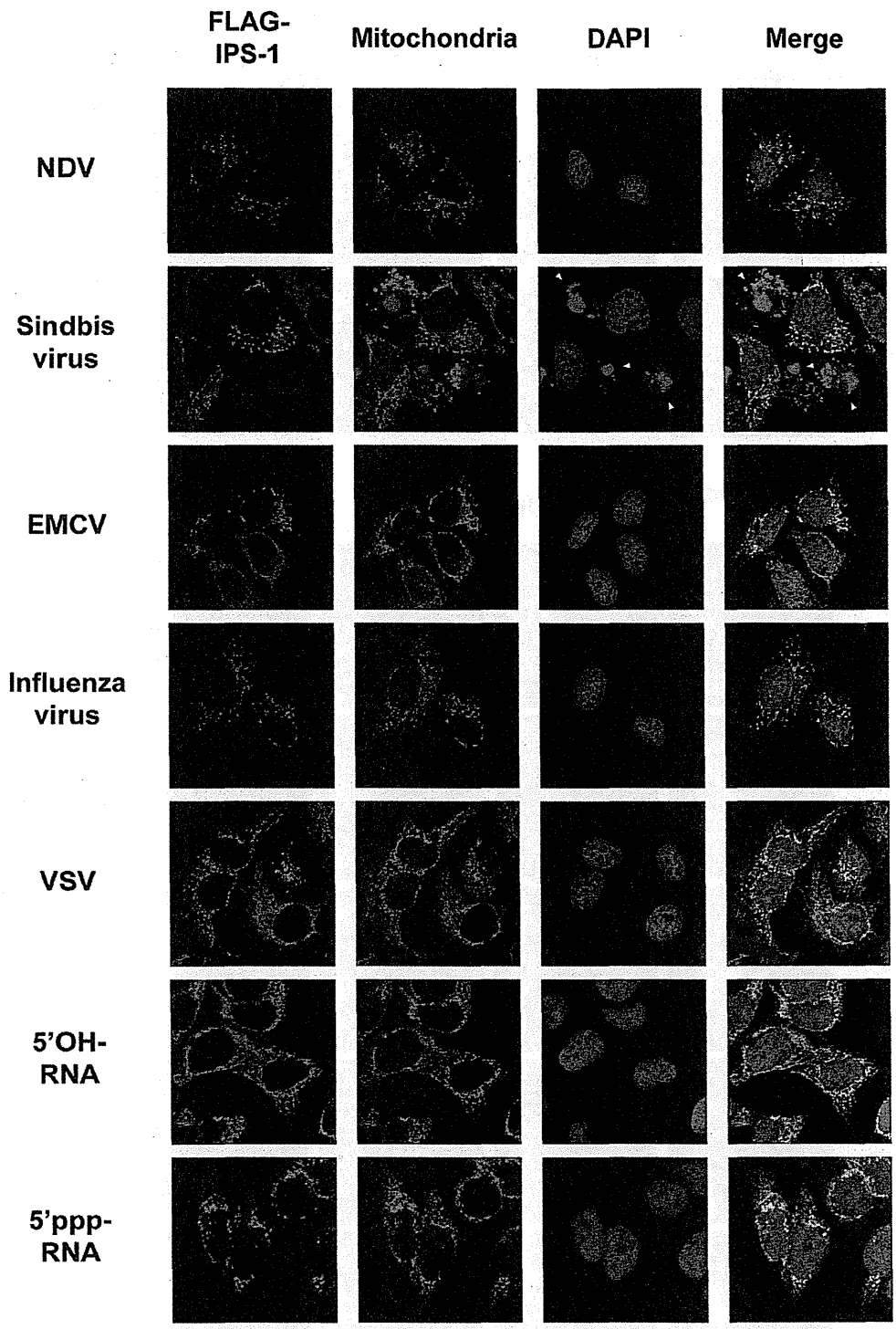

Figure 3. Redistribution of IPS-1 induced by virus-infection and 5′ppp-RNA-transfection. IPS-1-HeLa cells were infected with the indicated viruses or transfected with 5′OH-RNA or 5′ppp-RNA chemically synthesized by in vitro transcription using T7 RNA polymerase. At 12 h post-infection or -transfection, the cells were stained with anti-FLAG antibody and MitoTracker (Mitochondria). Arrowheads show dead cells with shrunk nuclei in Sindbis virus-infected cells.
doi:10.1371/journal.ppat.1001012.g003

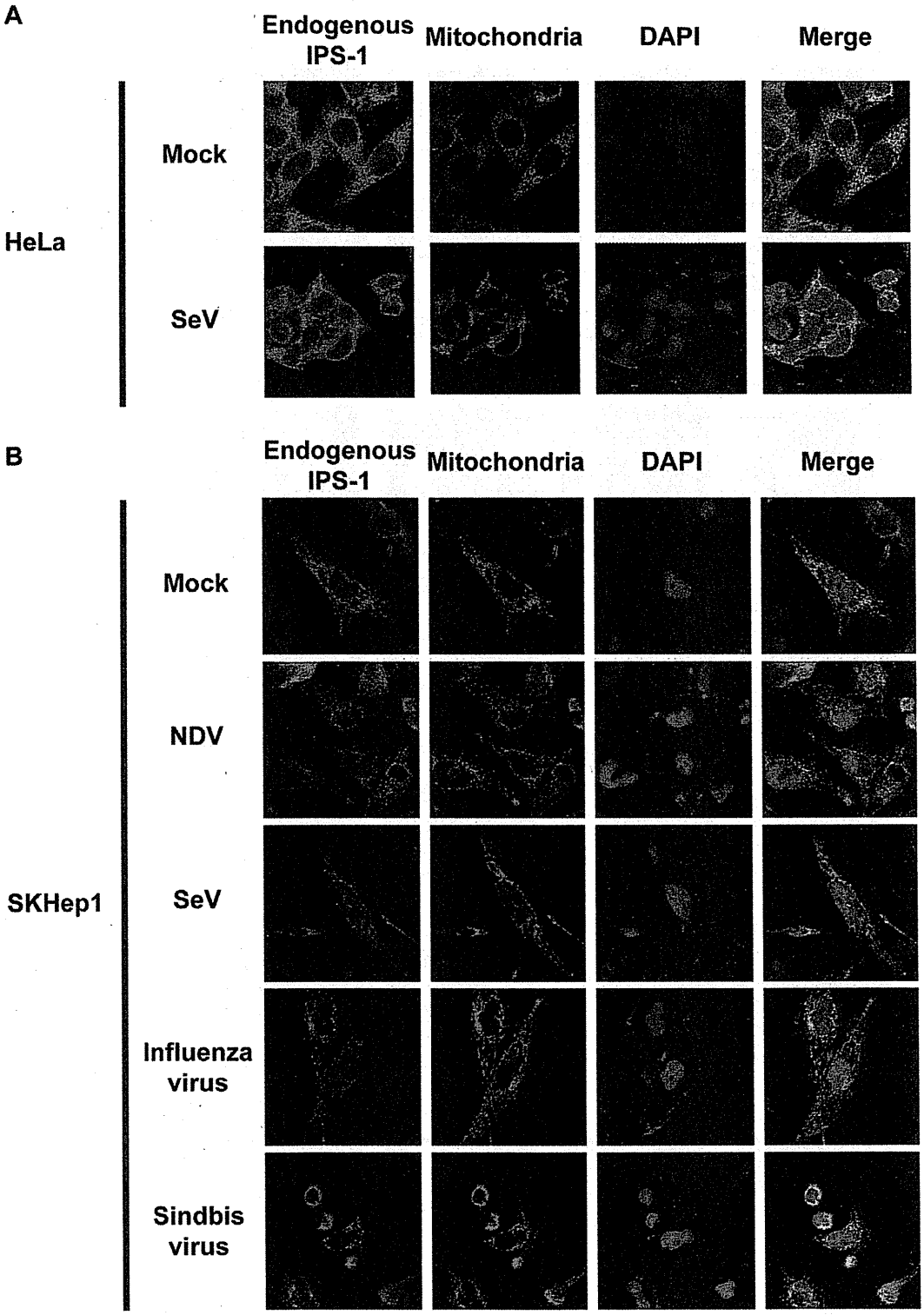

Figure 4. Redistribution of endogenous IPS-1 in virus-infected cells. A, HeLa cells were infected with Mock or SeV for 12 h. The cells were stained with anti-IPS-1 antibody and MitoTracker (Mitochondria). **B**, SKHep1 cells were infected with NDV, SeV, Influenza virus, or Sindbis virus for 12 h. The cells were stained with anti-IPS-1 antibody and MitoTracker (Mitochondria).
doi:10.1371/journal.ppat.1001012.g004

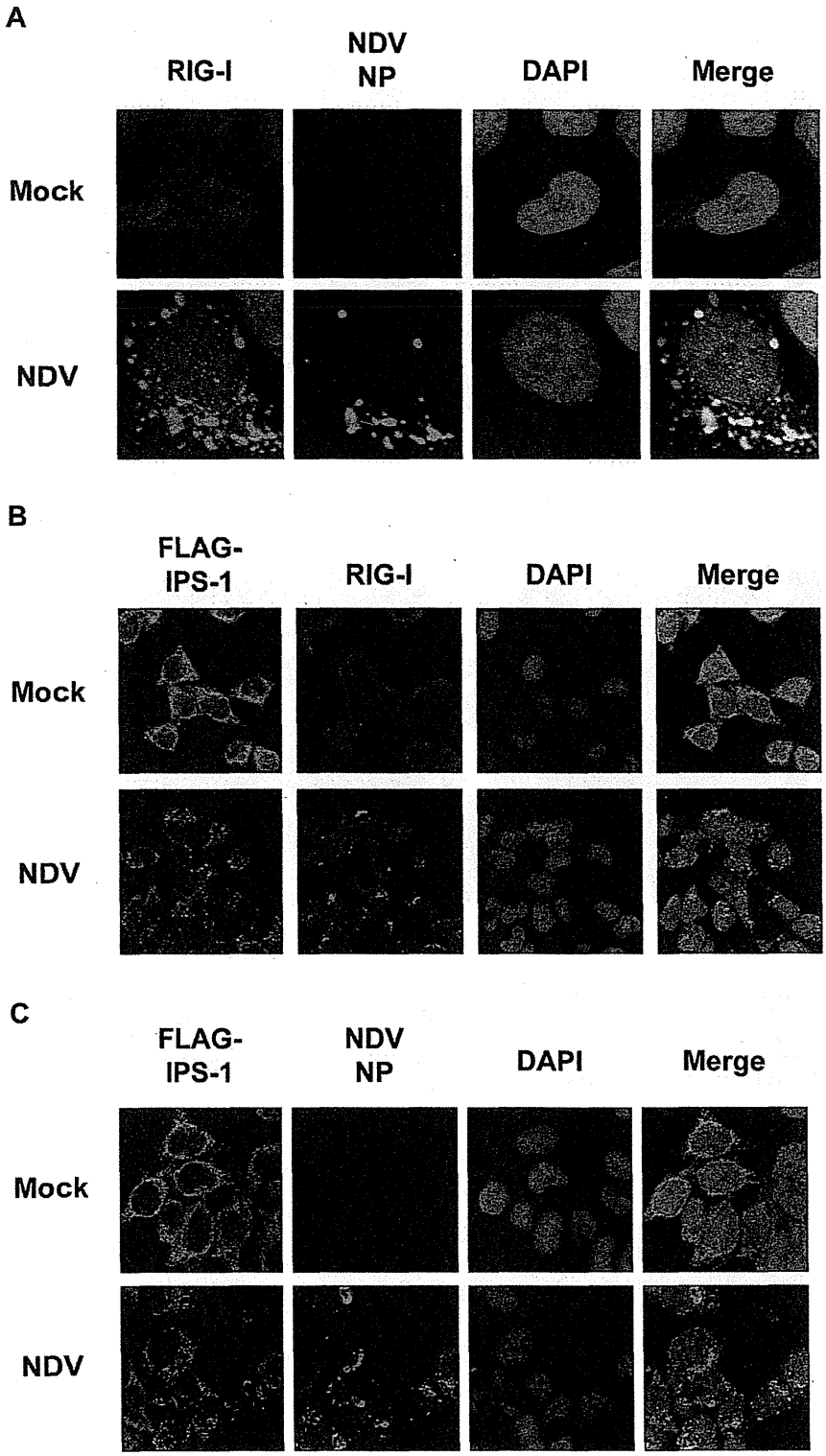

Figure 5. Localization of viral nucleocapsid, RIG-I, and IPS-1. A, HeLa cells were infected with NDV for 12 h and stained with anti-RIG-I antibody (RIG-I) and anti-NP antibody (NDV NP). **B** and **C**, IPS-1-HeLa cells were infected with NDV for 12 h and stained with anti-FLAG antibody and anti-RIG-I antibody or anti-NP antibody.
doi:10.1371/journal.ppat.1001012.g005

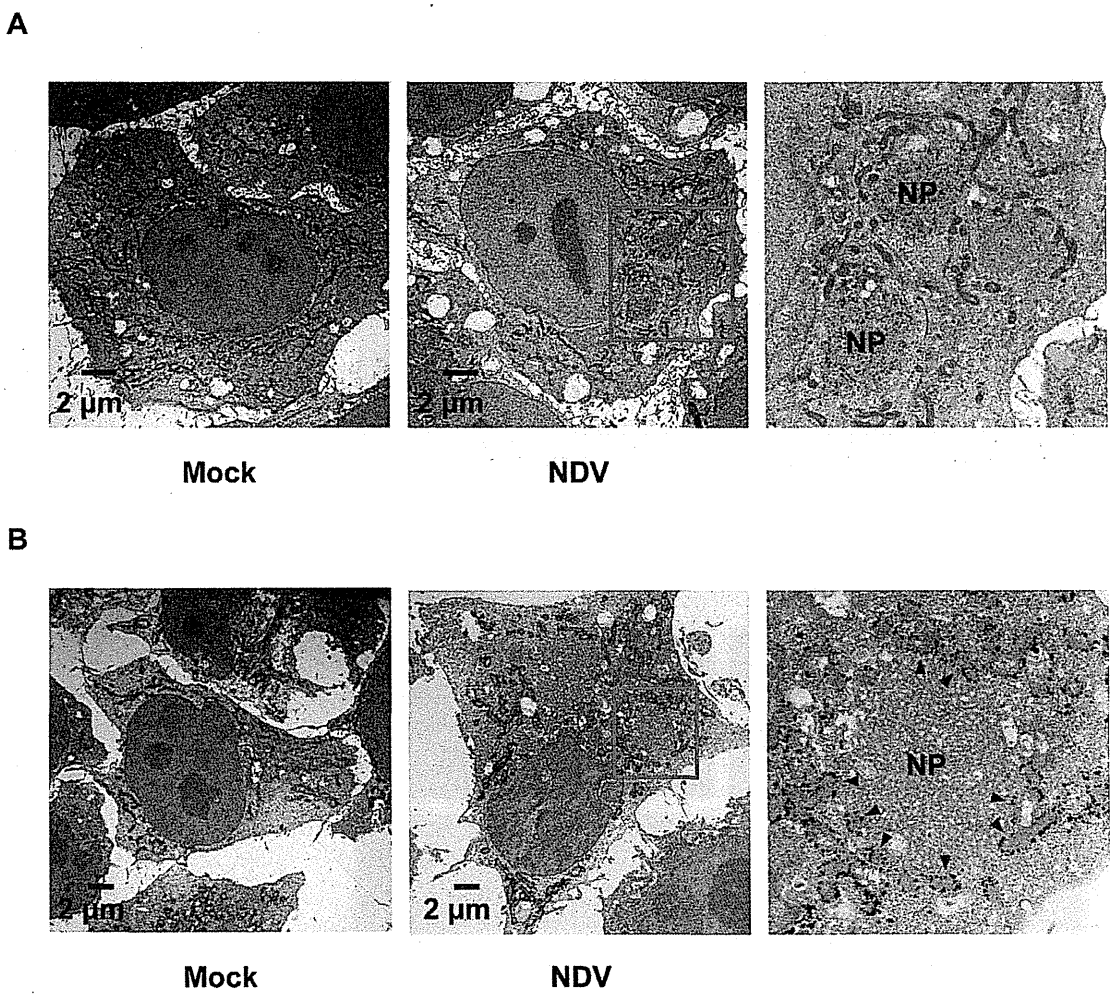

Figure 6. Localization of IPS-1 and mitochondria. A, IPS-1-HeLa cells infected with NDV for 9 h were fixed, stained with anti-NP antibody, and subjected to ultrathin sectioning as shown in the Methods. The area enclosed by a red rectangle is enlarged. NP: NP foci stained with the anti-NP antibody were visualized using gold particles. **B**, IPS-1-HeLa cells infected with NDV for 9 h were fixed, stained with anti-FLAG antibody, and subjected to ultra thin sectioning. The area enclosed by a red rectangle is enlarged. NP: morphologically similar structures are in **A**. IPS-1 was visualized using gold particles. The arrowheads indicate boundaries between IPS-1 and NP foci.
doi:10.1371/journal.ppat.1001012.g006

expressed on, and implicated in the fusion of the mitochondrial inner membrane [20]. Three independent siRNA targeting OPA1, down-regulated OPA1 expression (Fig. 9C) and partially (up to 50%) blocked NDV-induced signaling (Fig. 9D). However, the knockdown of dynamin-related protein 1 (DRP1) (Fig. 9E), which regulates mitochondrial fission [21] resulting in elongated mitochondria, did not have a significant effect (Fig. 9F). To explore the site where MFN1 is active, we temporarily overexpressed the dominant active RIG-I (RIG-I CARD) [17] or IPS-1 in wt and Mfn-knockout MEFs. Unlike the signal generated by the overexpression of IPS-1, the signal generated by overexpression of the RIG-I tandem caspase recruitment domain (CARD) clearly required MFN1. MFN1 however, is dispensable if IPS-1 is overexpressed (Fig. 9G). Again, MFN2 exhibited little influence on the signaling triggered by either stimulus. These results indicate that MFN1, but not MFN2, is essential for signal transduction mediated by RIG-I and IPS-1.

Physical interaction between IPS-1 and MFN1

To explore the molecular mechanism of how IPS-1 is regulated by MFN1, co-immunoprecipitation was performed using cells stably expressing IPS-1. FLAG-IPS-1 was precipitated by anti-FLAG and the associated proteins were analyzed by immunoblotting (Fig. 10). Both MFN1 and MFN2 constitutively associated with IPS-1 in the cells, but an unrelated mitochondrial outer membrane protein, BCL-XL, did not associate with IPS-1. Furthermore, OPA1 and DRP1 did not co-immunoprecipitate with FLAG-IPS-1. These data suggest that IPS-1 selectively associates with MFN1 and MFN2.

Knockdown of MFN1 inhibits the redistribution of IPS-1 induced by viral infection

Next, we examined what effect the knockdown of MFN1 would have on the virus-induced redistribution of IPS-1. Three independent siRNA efficiently knocked down MFN1 expression

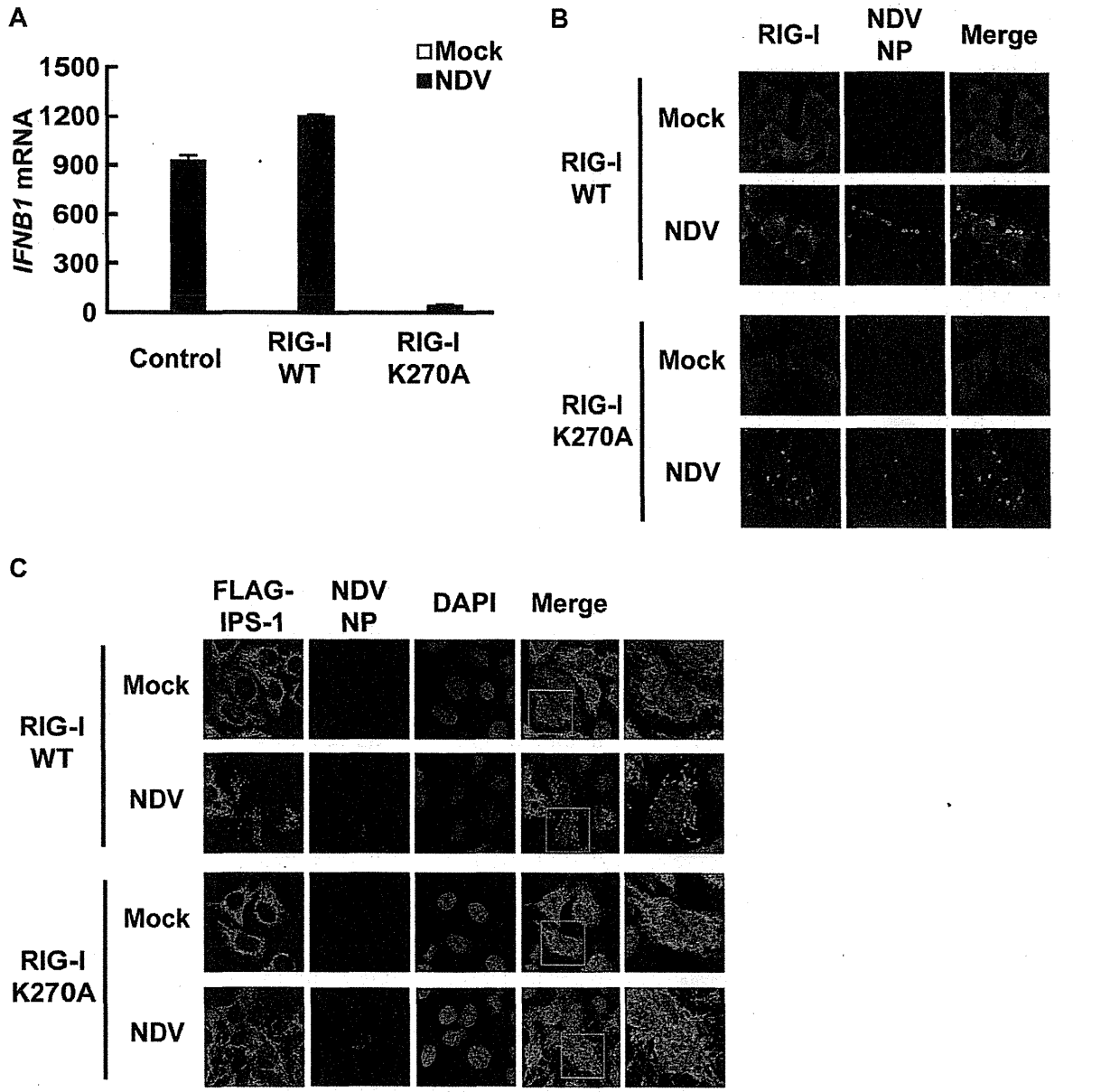

Figure 7. A dominant negative mutant of RIG-I fails to induce IPS-1 redistribution. A, IPS-1-HeLa cells stably expressing wild-type human RIG-I (RIG-I WT) or mutant RIG-I (RIG-I K270A) were mock-treated or infected with NDV for 12 h and expression of *IFNB1* mRNA was analyzed by qRT-PCR. Open and filled bars indicate RNA samples from mock-treated and NDV-infected cells, respectively. Data represent means ± s.d. (n = 3). **B**, IPS-1-HeLa cells expressing RIG-I WT or RIG-I K270A were infected with NDV for 12 h and stained with anti-RIG-I antibody and anti-NP antibody. RIG-I staining is diffuse in uninfected cells however infection by NDV produced RIG-I foci. Some RIG-I foci are co-localized with NDV NP foci. **C**, IPS-1-HeLa cells expressing RIG-I WT or RIG-I K270A were infected with NDV for 12 h and IPS-1 redistribution was examined. IPS-1 and NP were stained with anti-IPS-1 antibody and anti-NP antibody, respectively. The area enclosed by the red rectangle is enlarged at the right. Although the redistributed IPS-1 surrounds NP foci in RIG-I WT cells, K270A mutation of RIG-I failed to induce the redistribution of IPS-1, but not the formation of NP foci.
doi:10.1371/journal.ppat.1001012.g007

(Fig. 11A) resulting in a strong inhibition of the NDV-induced IFN-β gene expression in HeLa cells and IPS-1-HeLa cells (Fig. 11B and 11C). This once again suggests that IPS-1-HeLa cells tend to behave like normal cells. Upon NDV infection, IPS-1 displayed a speckled staining pattern in control cells, but not in the MFN1-knockdown cells (Fig. 11D). Though the intensity of NP staining did not increase, MFN1-knockdown significantly inhibited IFN gene activation. This correlates with prior observations that although IFN production is inhibited by LGP2 overexpression, viral yield does not increase [22]. When control siRNA-treated cells were infected with NDV, a redistribution of IPS-1 was observed (69.3±15.7% of cells positive for NP). In MFN1-knockdown cells, although NDV infection resulted in the formation of NP foci, IPS-1 redistribution did not occur

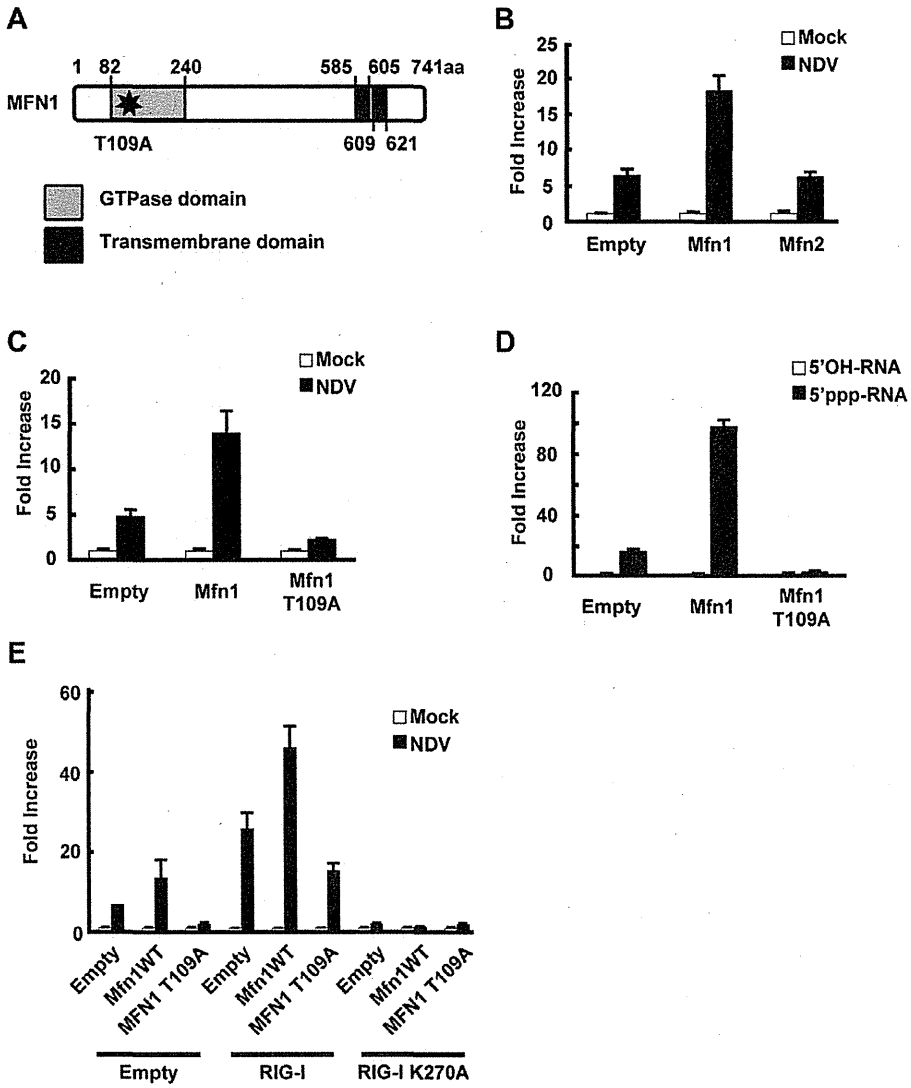

Figure 8. MFN1 is involved in antiviral signaling. A, Schematic representation of the MFN1 domain. **B**, L929 cells were transfected with a virus-responsive reporter gene (p-125 Luc) and either an empty vector (Empty), an expression vector for MFN1, or an expression vector for MFN2 as indicated. 48 h after the transfection, cells were mock-treated or infected with NDV. Luciferase activity was determined at 12 h after infection. **C** and **D**, L929 cells were transfected with a virus-responsive reporter gene (p-125 Luc) and either an empty vector (Empty) or an expression vector for MFN1 or its mutant (MFN1 T109A) as indicated. At 48 h after transfection, cells were mock-treated, infected with NDV, or transfected with 5'OH-RNA or 5'ppp-RNA. Luciferase activity was determined at 12 h (**C**) or 9 h (**D**) after induction. **E**, L929 cells were transfected with a virus-responsive reporter gene (p-125 Luc) and combinations of the indicated vectors. 48 h after the transfection, cells were mock-treated or infected with NDV. Luciferase activity was determined 12 h after infection.
doi:10.1371/journal.ppat.1001012.g008

(4.5±1.3% of cells positive for NP). A similar effect was observed when MFN1-knockdown cells were infected with SeV (Fig. 12). These results strongly suggest that MFN1 is critical to the redistribution of IPS-1 triggered by RIG-I mediated sensing of viral RNA.

Discussion

RIG-I mediated antiviral signaling is a critical antiviral response which is initiated when the RIG-I sensor recognizes viral RNA. A signal is relayed to IPS-1, a mitochondrial regulator which delivers the signal downstream. Interestingly, the IPS-1-HeLa clones in this study exhibited very low basal expression of IFN genes, which led us to speculate that IPS-I inhibitory protein(s) is up regulated in these clones. We also examined the expression level of NLRX1, an IPS-1 inhibitor [23], and noted no change in its expression level (not shown). Similarly, levels of MFN1 and MFN2 did not change in the IPS-1-HeLa clones. (Fig. 10, input).

We observed that the IPS-1 level did not change for up to 12 h in virus-infected cells and no specific modification of IPS-1 was identified up to that point. We therefore hypothesize that the activation status of IPS-1 is determined by its localization pattern. We speculate that the mechanism of mitochondrial fusion is mediated by MFN1, and that IPS-1 translocates from some

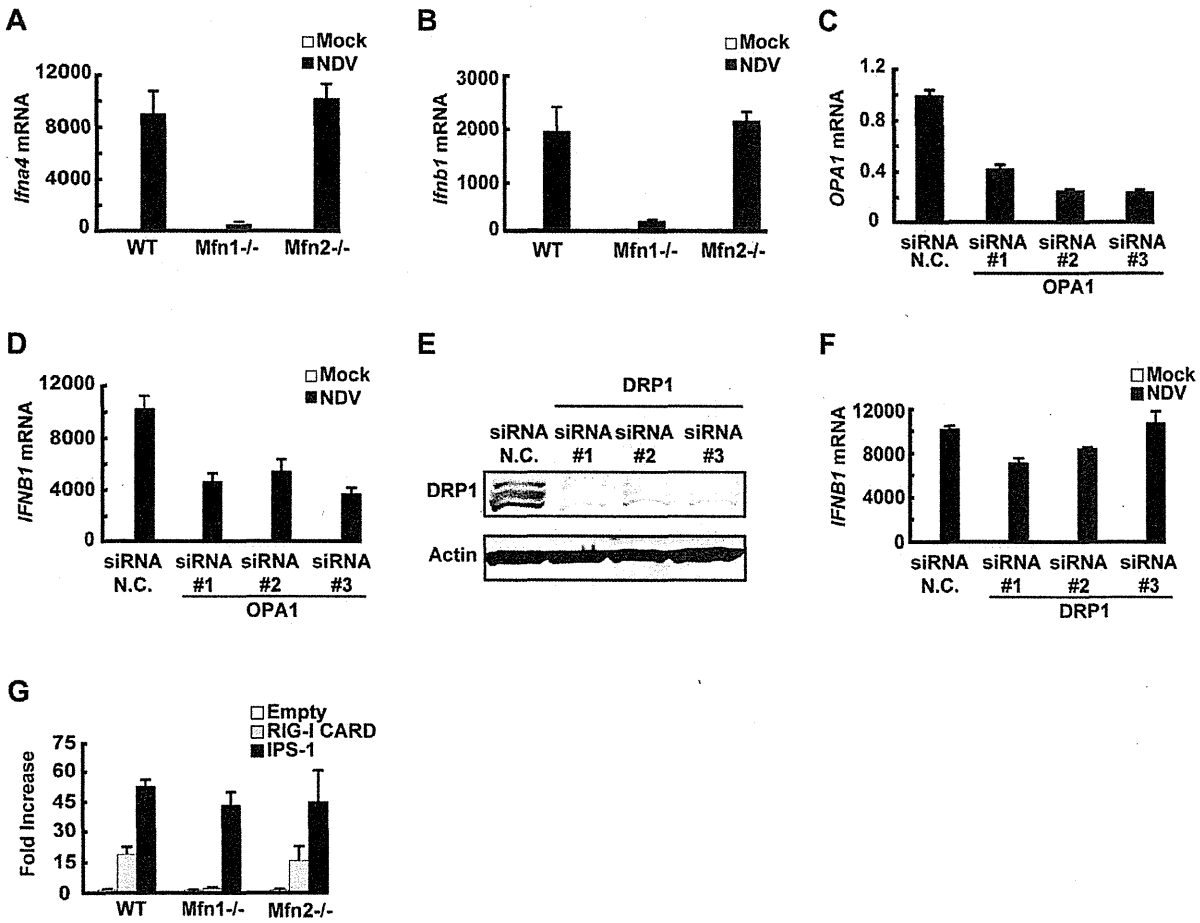

Figure 9. MFN1 plays a critical role in RIG-I–induced signaling. A and **B**, Wild-type (WT) MEFs and Mfn1 or Mfn2-knockout MEFs were infected with NDV for 9 h. The levels of endogenous *Ifna4* (**A**) and *Ifnb1* (**B**) mRNA were quantified by qRT-PCR. **C**, HeLa cells were transfected with negative control (N.C.) or hOPA1-targeted siRNA (#1–#3) for 72 h, and the expression of *OPA1* mRNA was analyzed by qRT-PCR. **D**, HeLa cells were transfected with N.C. siRNA or hOPA1-targeted siRNA. 72 h after transfection, cells were infected with NDV for 12 h. *IFNB1* mRNA expression was quantified by qRT-PCR. **E**, HeLa cells were transfected with N.C. siRNA or hDRP1-targeted siRNA (#1–#3) for 72 h, and the knockdown of endogenous DRP1 was analyzed by Western blotting using anti-DRP1 antibody. **F**, HeLa cells were transfected with N.C. siRNA or hDRP1-targeted siRNA. At 72 h after transfection, cells were infected with NDV for 12 h. *IFNB1* mRNA expression was quantified by qRT-PCR. **G**, WT and Mfn1 or Mfn2-knockout MEFs were transfected with a virus-responsive reporter gene (p-125 Luc) with either an empty vector (Empty) or an expression vector for RIG-I CARD or IPS-1. Luciferase activity was determined 48 h after transfection. Data represent means ± s.d. (n = 3).
doi:10.1371/journal.ppat.1001012.g009

mitochondria and finally accumulates densely on others. On the other hand, forced overexpression of full-length IPS-1 results in constitutive signaling [7,8,9,10]. There is no clear explanation why non-physiological overexpression can by-pass the virus-induced signaling, however, it can be concluded that transient IPS-1 overexpression may quantitatively override the hypothetical inhibitor for IPS-1 (above). Under these conditions, MFN1 is dispensable (Fig. 9G). Consistent with this, artificial aggregation of IPS-1 by cross-linking induced the signaling to activate IFN genes (Tang, E. D. and Wang, C. D. [24] and our unpublished observation). We speculate that under physiological conditions, viral infection induces the local accumulation of IPS-1 (corresponds to "active IPS-1") on mitochondria. These mitochondria with locally accumulated IPS-1 may function as a platform to recruit downstream molecules.

MFN1 and MFN2 are structurally similar and both occur on the outer membrane of mitochondria. Their functions however are not redundant, as the single knockout of either produces a certain mitochondrial phenotype [19]. Recently two papers were published concerning MFN function in RIG-I-mediated antiviral responses. Yasukawa et al. reported that MFN2 strongly interacts with IPS-1 thereby blocking its function, however MFN1 does not interact with IPS-1 and exhibits no effect [25]. These observations are clearly inconsistent with ours. The report by Castanier et al. however, is consistent with our finding that MFN1, but not MFN2, positively regulates IPS-1 [26]. Most importantly, our knockout results are clearly consistent with their knockdown results (Fig. 9A and B). Castanier et al. observed that a particular variant of SeV (H4) causes elongation of mitochondria, however they did not demonstrate whether this morphological change is common to other viral infections. Unlike Castanier et al. we did not observe mitochondrial elongation by viral infections nor 5′-pppRNA transfection (Fig. 3). The knockdown of a mitochondrial inner membrane protein OPA1 blocked virus-induced signaling

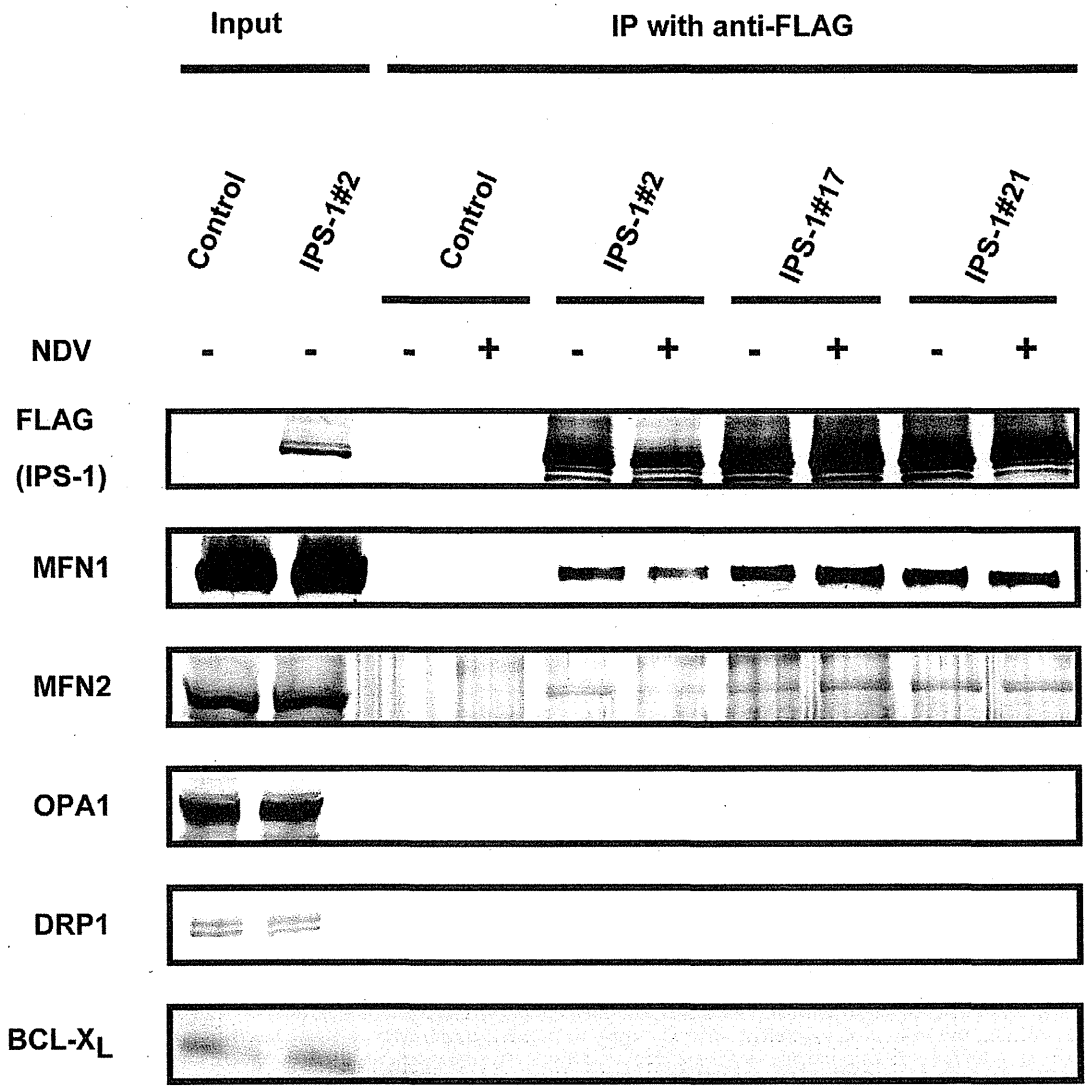

Figure 10. IPS-1 interacts with MFN1 and MFN2. IPS-1-HeLa cells were infected with NDV for 12 h, and then FLAG-IPS-1 was immunoprecipitated with anti-FLAG antibody. Co-immunoprecipitated MFN1 and MFN2 were detected by anti-MFN1 antibody and anti-MFN2 antibody, respectively. Neither OPA1 nor DRP1 was co-immunoprecipitated with FLAG-IPS-1. Mitochondrial protein BCL-XL was used as a control and was also examined by anti-BCLXL antibody.
doi:10.1371/journal.ppat.1001012.g010

(Fig. 9D); thereby indicating that mitochondrial fusion may be necessary for the activation of IPS-1. Castanier et al. observed that knockdown of DRP1 or FIS1 causes mitochondrial elongation and IPS-1's association with STING, an antiviral signaling adaptor. However, neither the mitochondrial elongation nor the IPS-1-STING interaction is sufficient to activate the signaling.

We demonstrated that the redistribution of IPS-1 is induced by various viral infections and 5′ppp-RNA transfection and is dependent on a functional MFN1. The precise mechanism of the IPS-1 redistribution is not known, however we propose a model described in Fig. 13. In uninfected cells, MFN1 and IPS-1 associate constitutively (Fig. 10) and distribute evenly on all mitochondria. When a virus replicates in a specific cytoplasmic compartment, RIG-I is recruited to this area as a result of interaction with viral dsRNA through the C-terminal RNA-binding domain (Fig. 5A). Upon binding with viral RNA, CARD is exposed (activate RIG-I) [27], and then interacts with IPS-1 at the periphery of the viral compartment. At the same time, mitochondria surround the viral compartment because it lacks the ability to penetrate it (Fig. 6). Since mitochondrion is an elastic, movable organelle [28], affinity between RIG-I and IPS-1 may be sufficient for the mitochondrial relocalization. IPS-1/MFN1 complex may facilitate fusion between the surrounding mitochondria. Mitochondrial fission occurs independently to balance the fusion, however since the fusion of IPS-1/MFN1-enriched mitochondria facilitates the redistribution of IPS-1, IPS-1-enriched mitochondria may be generated. Further research is necessary to elucidate if the mitochondrial fusion process is indeed central to IPS-1 redistribution.

In summary, our study provides new insight into why the mitochondrial localization of IPS-1 is essential to its function. We

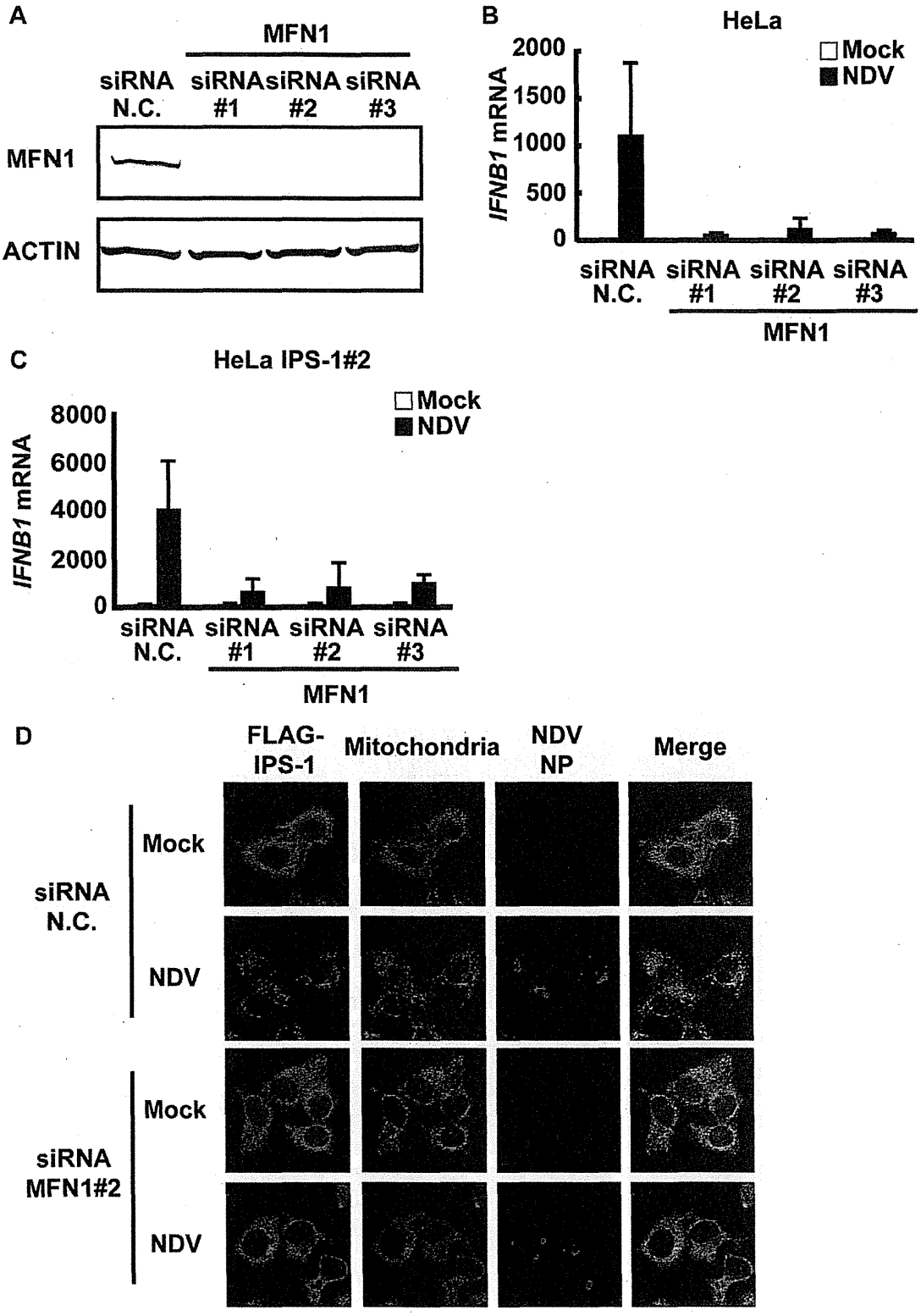

Figure 11. Knockdown of MFN1 inhibits the redistribution of IPS-1 induced by NDV infection. A, HeLa cells were transfected with negative control (N.C.) or hMFN1-targeted siRNA (#1–#3) for 48 h, and the knockdown of endogenous MFN1 was analyzed by Western blotting using anti-MFN1 antibody. **B**, Cells transfected with siRNA as shown in **a** were infected with NDV for 12 h, and endogenous *IFNB1* mRNA expression